PACIFIC EARTHQUAKE ENGINEERING
RESEARCH CENTER

PB99-157679

Capacity-Demand-Diagram Methods for Estimating Seismic Deformation of Inelastic Structures: SDF Systems

Anil K. Chopra
University of California
Berkeley

Rakesh K. Goel
California State Polytechnic University
San Luis Obispo

A report on research conducted under
grant no. CMS-9812531 from the National Science Foundation:
U.S. Japan Coooperative Research in Urban Earthquake Disaster Mitigation

R 1999/02
RIL 1999

Disclaimer

The opinions, findings, and conclusions or recommendations expressed in this publication are those of the author(s) and do not necessarily reflect the views of the study sponsor(s) or the Pacific Earthquake Engineering Research Center.

50272-101

REPORT DOCUMENTATION PAGE	1. REPORT NO. PEER 1999/02	2.	3. Recipient's Accession No.

4. Title and Subtitle CAPACITY-DEMAND-DIAGRAM METHODS FOR ESTIMATING SEISMIC DEFORMATION OF INELASTIC STRUCTURES: SDF SYSTEMS

5. Report Date April 1999/02

6.

7. Author(s) Anil K. Chopra, Rakesh K. Goel

8. Performing Organization Rept. No. PEER 1999/02

9. Performing Organization Name and Address

PACIFIC EARTHQUAKE ENGINEERING RESEARCH CENTER
1301 46th STREET
RICHMOND, CA 94804-4698

PB99-157679

10. Project/Task/Work Unit No.

11. Contract(C) or Grant(G) No.

(C)

(G) CMS-981231

12. Sponsoring Organization Name and Address

National Science Foundation
1800 G. Street, N.W.
Washington, D.C. 20550

13. Type of Report & Period Covered Final

14.

15. Supplementary Notes

16. Abstract (Limit: 200 words)

The ATC-40 and FEMA-274 documents contain simplified nonlinear analysis procedures to determine the displacement demand imposed on a building expected to deform inelastically. The Nonlinear Static Procedure in these documents, based on the capacity spectrum method, involves several approximations: The lateral force distribution for pushover analysis and conversion of these results to the capacity diagram are based only on the fundamental vibration mode of the elastic system. The earthquake-induced deformation of an inelastic SDF system is estimated by an iterative method requiring analysis of a sequence of equivalent linear systems, thus avoiding the dynamic analysis of the inelastic SDF system. This last approximation is first evaluated in this report, followed by the development of an improved simplified analysis procedure, based on capacity and demand diagrams, to estimate the peak deformation of inelastic SDF systems.

Several deficiencies in ATC-40 Procedure A are demonstrated. This iterative procedure did not converge for some of the systems analyzed. It converged in many cases, but to a deformation much different than dynamic (nonlinear response history or inelastic design spectrum) analysis of the inelastic system. The ATC-40 Procedure B always gives a unique value of deformation, the same as that determined by Procedure A if it converged.

The peak deformation of inelastic systems determined by ATC-40 procedures are shown to be inaccurate when compared against results of nonlinear response history analysis and inelastic design spectrum analysis. The approximate procedure underestimates significantly the deformation for a wide range of periods and ductility factors with errors approaching 50%, implying that the estimated deformation is about half the "exact" value.

Surprisingly, the ATC-40 procedure is deficient relative to even the *elastic* design spectrum in the velocity-sensitive and displacement-sensitive regions of the spectrum. For periods in these regions, the peak deformation of an inelastic system can be estimated from the elastic design spectrum using the well-known equal displacement rule. However, the approximate procedure requires analyses of several equivalent linear systems and still produces worse results.

Finally, an improved capacity-demand-diagram method that uses the well-known constant-ductility design spectrum for the demand diagram has been developed and illustrated by examples. This method gives the deformation value consistent with the selected inelastic design spectrum, while retaining the attraction of graphical implementation of the ATC-40 methods. One version of the improved method is graphically similar to ATC-40 Procedure A whereas a second version is graphically similar to ATC-40 Procedure B. However, the improved procedures differ from ATC-40 procedures in one important sense. The demand is determined by analyzing an inelastic system in the improved procedure instead of equivalent linear systems in ATC-40 procedures.

The improved method can be conveniently implemented numerically if its graphical features are not important to the user. Such a procedure, based on equations relating R_y and μ for different T_n ranges, has been presented, and illustrated by examples using three different $R_y-\mu-T_n$ relations.

17. Document Analysis a. Descriptors

b. Identifiers/Open-Ended Terms

c. COSATI Field/Group

18. Availability Statement: No restrictions. This document is available to the public through the National Technical Service, Springfield, VA 22161.	19. Security Class (This Report) Unclassified	21. No. of Pages 72
	20. Security Class (This Page) Unclassified	22. Price

(See ANSI-Z39.18) *See Instructions on Reverse*

OPTIONAL FORM 272 (4-77)
(Formerly NTIS-35)
Department of Commerce

Capacity-Demand-Diagram Methods for Estimating Seismic Deformation of Inelastic Structures: SDF Systems

Anil K. Chopra
University of California
Berkeley

Rakesh K. Goel
California State Polytechnic University
San Luis Obispo

A report on research conducted under
grant no. CMS-9812531 from the National Science Foundation:
U.S.-Japan Cooperative Research in Urban Earthquake Disaster Mitigation

PEER-1999/02
Pacific Earthquake Engineering Research Center
College of Engineering
University of California, Berkeley

April 1999

ABSTRACT

The ATC-40 and FEMA-274 documents contain simplified nonlinear analysis procedures to determine the displacement demand imposed on a building expected to deform inelastically. The Nonlinear Static Procedure in these documents, based on the capacity spectrum method, involves several approximations: The lateral force distribution for pushover analysis and conversion of these results to the capacity diagram are based only on the fundamental vibration mode of the elastic system. The earthquake-induced deformation of an inelastic SDF system is estimated by an iterative method requiring analysis of a sequence of equivalent linear systems, thus avoiding the dynamic analysis of the inelastic SDF system. This last approximation is first evaluated in this report, followed by the development of an improved simplified analysis procedure, based on capacity and demand diagrams, to estimate the peak deformation of inelastic SDF systems.

Several deficiencies in ATC-40 Procedure A are demonstrated. This iterative procedure did not converge for some of the systems analyzed. It converged in many cases, but to a deformation much different than dynamic (nonlinear response history or inelastic design spectrum) analysis of the inelastic system. The ATC-40 Procedure B always gives a unique value of deformation, the same as that determined by Procedure A if it converged.

The peak deformation of inelastic systems determined by ATC-40 procedures are shown to be inaccurate when compared against results of nonlinear response history analysis and inelastic design spectrum analysis. The approximate procedure underestimates significantly the deformation for a wide range of periods and ductility factors with errors approaching 50%, implying that the estimated deformation is about half the "exact" value.

Surprisingly, the ATC-40 procedure is deficient relative to even the *elastic* design spectrum in the velocity-sensitive and displacement-sensitive regions of the spectrum. For periods in these regions, the peak deformation of an inelastic system can be estimated from the elastic design spectrum using the well-known equal displacement rule. However, the approximate procedure requires analyses of several equivalent linear systems and still produces worse results.

Finally, an improved capacity-demand-diagram method that uses the well-known constant-ductility design spectrum for the demand diagram has been developed and illustrated by examples. This method gives the deformation value consistent with the selected inelastic design spectrum, while retaining the attraction of graphical implementation of the ATC-40 methods. One version of the improved method is graphically similar to ATC-40 Procedure A whereas a second version is graphically similar to ATC-40 Procedure B. However, the improved procedures differ from ATC-40 procedures in one important sense. The demand is determined by analyzing an inelastic system in the improved procedure instead of equivalent linear systems in ATC-40 procedures.

The improved method can be conveniently implemented numerically if its graphical features are not important to the user. Such a procedure, based on equations relating R_y and μ for different T_n ranges, has been presented, and illustrated by examples using three different $R_y - \mu - T_n$ relations.

ACKNOWLEDGMENTS

This research investigation is funded by the National Science Foundation under Grant CMS-9812531, a part of the U.S.-Japan Cooperative Research in Urban Earthquake Disaster Mitigation. This financial support is gratefully acknowledged. Dr. Rakesh Goel acknowledges the State Faculty Support Grant Fellowship received during summer of 1998.

The authors have benefited from discussions with Chris D. Poland and Wayne A. Low, who are working on a companion research project awarded to Degenkolb Engineers; and with Sigmund A. Freeman, who, more than any other individual, has been responsible for the concept and development of the capacity spectrum method.

CONTENTS

INTRODUCTION

A major challenge to performance-based seismic design and engineering of buildings is to develop simple, yet effective, methods for designing, analyzing and checking the design of structures so that they reliably meet the selected performance objectives. Needed are analysis procedures that are capable of predicting the demands — forces and deformations — imposed by earthquakes on structures more realistically than has been done in building codes. In response to this need, simplified, nonlinear analysis procedures have been incorporated in the ATC-40 and FEMA-274 documents (Applied Technology Council, 1996; FEMA, 1997) to determine the displacement demand imposed on a building expected to deform inelastically.

The Nonlinear Static Procedure in these documents is based on the capacity spectrum method originally developed by Freeman et al. (1975) and Freeman (1978). It consists of the following steps:

1. Develop the relationship between base shear, V_b, and roof (Nth floor) displacement, u_N (Fig. 1a), commonly known as the pushover curve.
2. Convert the pushover curve to a capacity diagram, (Fig. 1b), where

$$\Gamma_1 = \frac{\sum_{j=1}^{N} m_j \phi_{j1}}{\sum_{j=1}^{N} m_j \phi_{j1}^2} \qquad M_1^* = \frac{\left(\sum_{j=1}^{N} m_j \phi_{j1}\right)^2}{\sum_{j=1}^{N} m_j \phi_{j1}^2} \tag{1}$$

   and m_j = lumped mass at the jth floor level, ϕ_{j1} is the jth-floor element of the fundamental mode ϕ_1, N is the number of floors, and M_1^* is the effective modal mass for the fundamental vibration mode.
3. Convert the elastic response (or design) spectrum from the standard pseudo-acceleration, A, versus natural period, T_n, format to the $A-D$ format, where D is the deformation spectrum ordinate (Fig. 1c).
4. Plot the demand diagram and capacity diagram together and determine the displacement demand (Fig. 1d). Involved in this step are dynamic analyses of a sequence of equivalent linear systems with successively updated values of the natural vibration period, T_{eq}, and equivalent viscous damping, $\hat{\xi}_{eq}$ (to be defined later).
5. Convert the displacement demand determined in Step 4 to global (roof) displacement and individual component deformation and compare them to the limiting values for the specified performance goals.

Approximations are implicit in the various steps of this simplified analysis of an inelastic MDF system. Implicit in Steps 1 and 2 is a lateral force distribution assumed to be fixed, and based only on the fundamental vibration mode of the elastic system; however, extensions to account for higher mode effects have been proposed (Paret et al., 1996). Implicit in Step 4 is the belief that the earthquake-induced deformation of an inelastic SDF system can be estimated

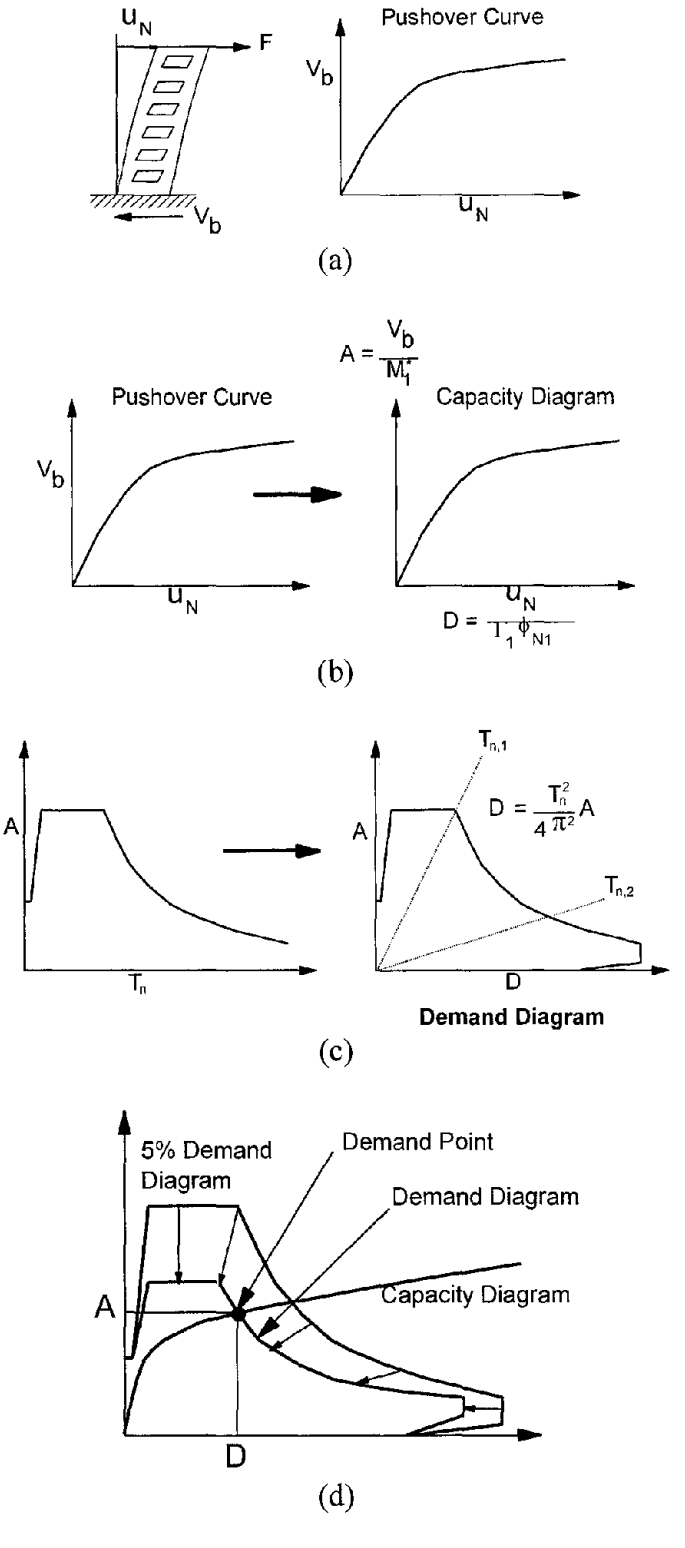

Figure 1. Capacity spectrum method: (a) development of pushover curve, (b) conversion of pushover curve to capacity diagram, (c) conversion of elastic response spectrum from standard format to A-D format, and (d) determination of displacement demand.

satisfactorily by an iterative method requiring analysis of a sequence of equivalent linear SDF systems, thus avoiding the dynamic analysis of the inelastic SDF system. This investigation focuses on the rationale and approximations inherent in this critical step.

The principal objective of this investigation is to develop improved simplified analysis procedures, based on capacity and demand diagrams, to estimate the peak deformation of inelastic SDF systems. The need for such procedures is motivated by first evaluating the above mentioned approximation inherent in Step 4 of the ATC-40 procedure. Thereafter, improved procedures using the well-established inelastic response (or design) spectrum (e.g., Chopra, 1995; Section 7.10) are developed. The idea of using the inelastic design spectrum in this context was suggested by Bertero (1995) and introduced by Reinhorn (1997) and Fajfar (1998, 1999); and the capacity spectrum method has been evaluated previously, e.g., Tsopelas et al. (1997).

EQUIVALENT LINEAR SYSTEMS

The earthquake response of inelastic systems can be estimated by approximate analytical methods in which the nonlinear system is replaced by an "equivalent" linear system. These methods attracted the attention of researchers in the 1960s before high speed digital computers were widely used for nonlinear analyses, and much of the fundamental work was accomplished over two decades ago (Hudson, 1965; Jennings, 1968; Iwan and Gates, 1979a). In general, approximate methods for determining the parameters of the equivalent linear system fall into two categories: methods based on harmonic response and methods based on random response. Six methods are available in the first category and three in the second category. Formulas for the natural vibration period and damping ratio are available for each method (Iwan and Gates, 1979a). Generally speaking, the methods based on harmonic response considerably overestimate the period shift, whereas the methods considering random response give much more realistic estimates of the period (Iwan and Gates, 1979b).

Now there is renewed interest in applications of equivalent linear systems to design of inelastic structures. For such applications, the secant stiffness method (Jennings, 1968) is being used in the capacity spectrum method to check the adequacy of a structural design (e.g., Freeman et al., 1975; Freeman, 1978; Deierlein and Hsieh, 1990; Reinhorn et al., 1995) and has been adapted to develop the "nonlinear static procedure" in the ATC-40 report (Applied Technology Council, 1996) and the FEMA-274 report (FEMA, 1997). A variation of this method, known as the substitute structure method (Shibata and Sozen, 1976), is popular for displacement-based design (Gulkan and Sozen, 1974; Shibata and Sozen, 1976; Moehle, 1992; Kowalsky et al., 1995; Wallace, 1995). Based on harmonic response, these two methods are known to be not as accurate as methods based on random response (Iwan and Gates, 1979a,b). The equivalent linear system based on the secant stiffness is reviewed next.

Consider an inelastic SDF system with bilinear force-deformation relationship on initial loading (Fig. 2a). The stiffness of the elastic branch is k and that of the yielding branch is αk. The yield strength and yield displacement are denoted by f_y and u_y, respectively. If the peak (maximum absolute) deformation of the inelastic system is u_m, the ductility factor $\mu = u_m/u_y$.

For the bilinear system of Fig. 2a, the natural vibration period of the equivalent linear system with stiffness equal to k_{sec}, the secant stiffness, is

$$T_{eq} = T_n \sqrt{\frac{\mu}{1+\alpha\mu-\alpha}} \tag{2}$$

where T_n is the natural vibration period of the system vibrating within its linearly elastic range ($u \le u_y$).

The most common method for defining equivalent viscous damping is to equate the energy dissipated in a vibration cycle of the inelastic system and of the equivalent linear system. Based on this concept, it can be shown that the equivalent viscous damping ratio is (Chopra, 1995: Section 3.9)

$$\zeta_{eq} = \frac{1}{4\pi}\frac{E_D}{E_S} \tag{3}$$

where the energy dissipated in the inelastic system is given by the area E_D enclosed by the hysteresis loop (Fig. 2b) and $E_S = k_{sec} u_m^2/2$ is the strain energy of the system with stiffness k_{sec} (Fig. 2b). Substituting for E_D and E_S in Eq. (3) leads to

$$\zeta_{eq} = \frac{2}{\pi}\frac{(\mu-1)(1-\alpha)}{\mu(1+\alpha\mu-\alpha)} \tag{4}$$

The total viscous damping of the equivalent linear system is

$$\hat{\zeta}_{eq} = \zeta + \zeta_{eq} \tag{5}$$

where ζ is the viscous damping ratio of the bilinear system vibrating within its linearly elastic range ($u \le u_y$).

For elastoplastic systems, $\alpha = 0$ and Eqs. (2) and (4) reduce to

$$T_{eq} = T_n\sqrt{\mu} \qquad \zeta_{eq} = \frac{2}{\pi}\frac{\mu-1}{\mu} \tag{6}$$

Equations (2) and (4) are plotted in Fig. 3 where the variation of T_{eq}/T_n and ζ_{eq} with μ is shown for four values of α. For yielding systems ($\mu > 1$), T_{eq} is longer than T_n and $\zeta_{eq} > 0$. The period of the equivalent linear system increases monotonically with μ for all α. For a fixed μ T_{eq} is longest for elastoplastic systems and is shorter for systems with $\alpha > 0$. For $\alpha = 0$, ζ_{eq} increases monotonically with μ but not for $\alpha > 0$. For the latter case, ζ_{eq} reaches its maximum value at a μ value, which depends on α, and then decreases gradually.

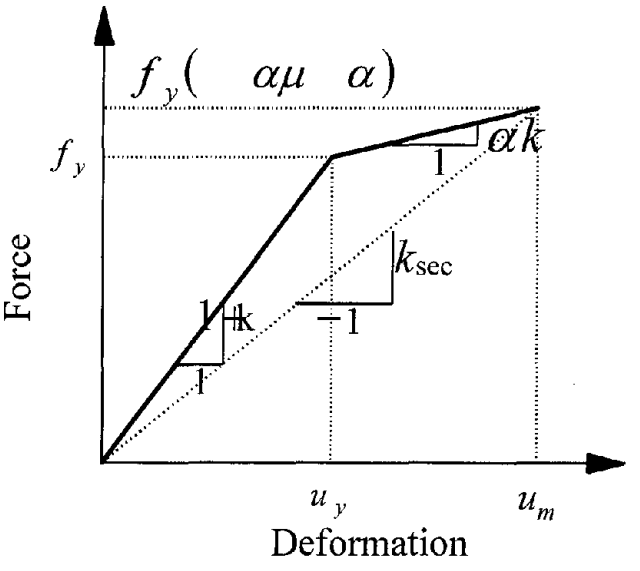

(a)

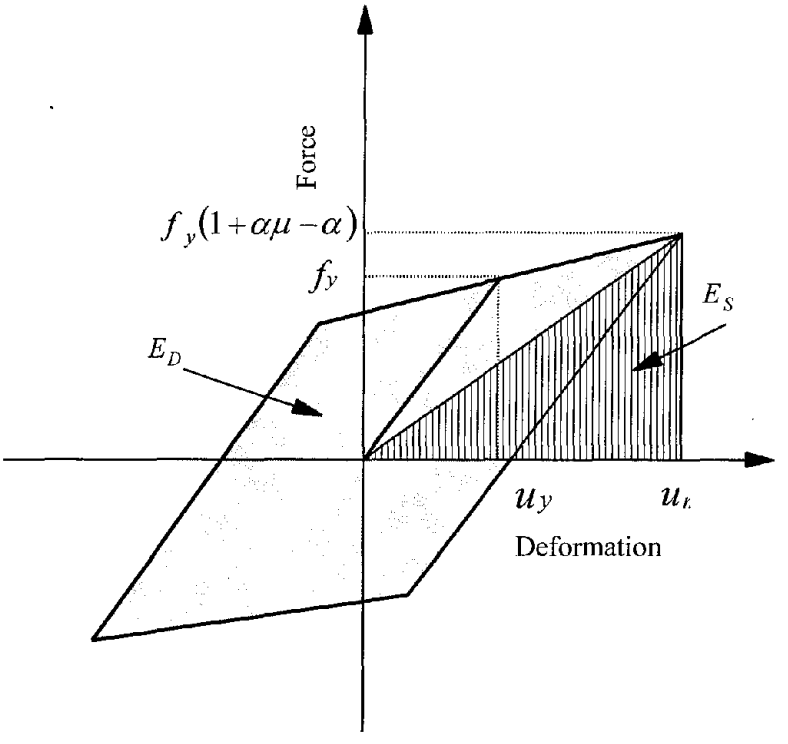

(b)

Figure 2. Inelastic SDF system: (a) bilinear force-deformation relationship; (b) equivalent viscous damping due to hysteretic energy dissipation.

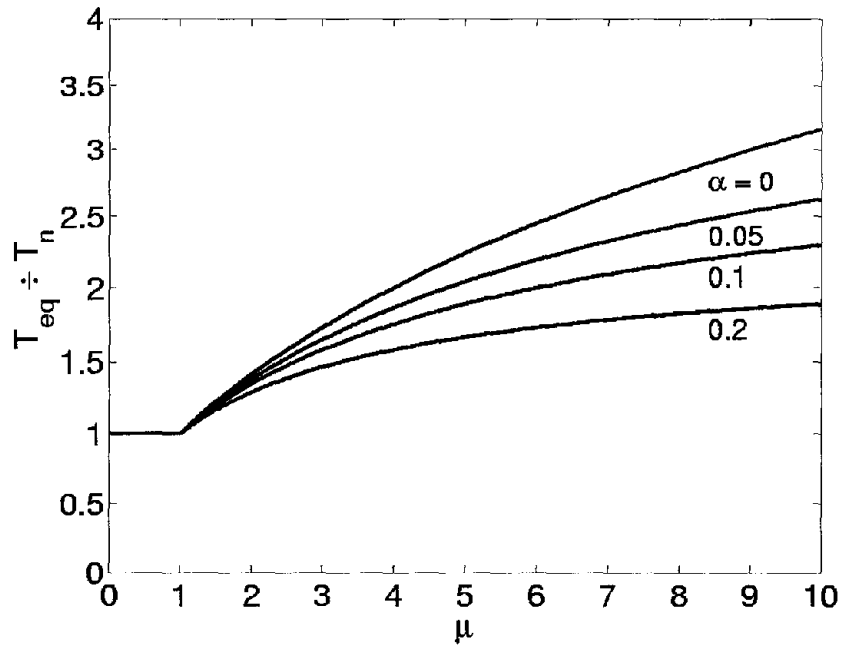

(a)

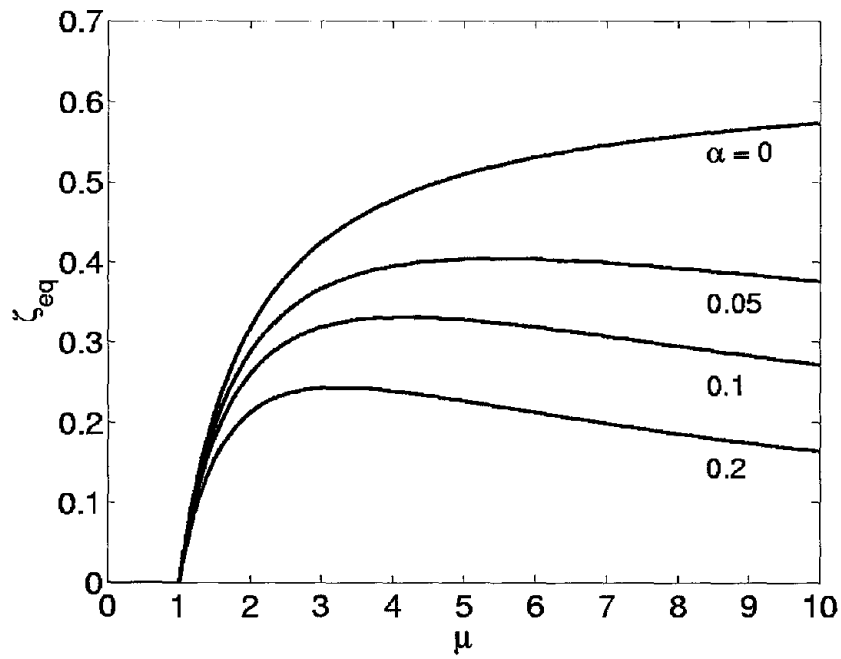

(b)

Figure 3. Variation of period and viscous damping of the equivalent linear system with ductility.

ATC-40 ANALYSIS PROCEDURES

Contained in the ATC-40 report are approximate analysis procedures to estimate the earthquake-induced deformation of an inelastic system. These procedures are approximate in the sense that they avoid dynamic analysis of the inelastic system. Instead dynamic analyses of a sequence of equivalent linear systems with successively updated values of T_{eq} and $\hat{\xi}_{eq}$ provide a basis to estimate the deformation of the inelastic system; T_{eq} is determined by Eq. (2) but $\hat{\xi}_{eq}$ by a modified version of Eq. (5):

$$\hat{\xi}_{eq} = \zeta + \kappa \zeta_{eq} \tag{7}$$

with ζ_{eq} limited to 0.45. Although the basis for selecting this upper limit on damping is not stated explicitly, ATC-40 states that "The committee who developed these damping coefficients concluded that spectra should not be reduced to this extent at higher values and judgmentally ... set an absolute limit on ... $[0.05+\zeta_{eq}]$ of about 50 percent."

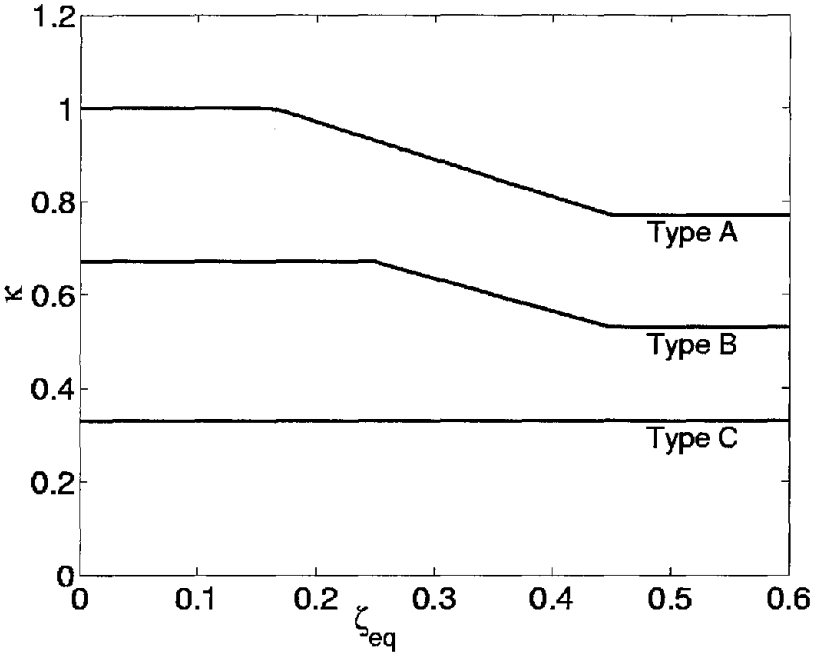

Figure 4. Variation of damping modification factor with equivalent viscous damping.

The damping modification factor, κ, based primarily on judgment, depends on the hysteretic behavior of the system, characterized by one of three types: Type A denotes hysteretic behavior with stable, reasonably full hysteresis loops, whereas Type C represents severely pinched and/or degraded loops; Type B denotes hysteretic behavior intermediate between Types A and C. ATC-40 contains equations for κ as a function of ζ_{eq} computed by Eq. (3) for the three types of hysteretic behavior. These equations, plotted in Fig. 4, were designed to ensure that κ does not exceed an upper limit, a requirement in addition to the limit of 45% on ζ_{eq}.

ATC-40 states that "... they represent the consensus opinion of the product development team." Concerned with bilinear systems, this paper will use the κ specified for Type A systems.

ATC-40 specifies three different procedures to estimate the earthquake-induced deformation demand, all based on the same underlying principles, but differing in implementation. Procedures A and B are analytical and amenable to computer implementation, whereas procedure C is graphical and most suited for hand analysis. Designed to be the most direct application of the methodology, Procedure A is suggested to be the best of the three procedures. The capacity diagram is assumed to be bilinear in Procedure B. The description of Procedures A and B that follows is equivalent to that in the ATC-40 report except that it is specialized for bilinear systems.

PROCEDURE A

This procedure in the ATC-40 report is described herein as a sequence of steps:

1. Plot the force-deformation diagram and the 5%-damped elastic response (or design) diagram, both in the $A-D$ format to obtain the capacity diagram and 5%-damped elastic demand diagram, respectively.
2. Estimate the peak deformation demand D_i and determine the corresponding pseudo-acceleration A_i from the capacity diagram. Initially, assume $D_i = D(T_n, \zeta = 5\%)$, determined for period T_n from the elastic demand diagram.
3. Compute ductility $\mu = D_i \div u_y$.
4. Compute the equivalent damping ratio $\hat{\zeta}_{eq}$ from Eq. (7).
5. Plot the elastic demand diagram for $\hat{\zeta}_{eq}$ determined in Step 4 and read-off the displacement D_j where this diagram intersects the capacity diagram.
6. Check for convergence. If $(D_j - D_i) \div D_j \leq$ tolerance (=0.05) then the earthquake induced deformation demand $D = D_j$. Otherwise, set $D_i = D_j$ (or another estimated value) and repeat Steps 3-6.

Examples: Specified Ground Motion

This procedure is used to compute the earthquake-induced deformation of the six example systems listed in Table 1. Considered are two values of T_n: 0.5s in the acceleration-sensitive spectral region and 1s in the velocity-sensitive region, and three levels of yield strength; ζ=5% for all systems. The excitation chosen is the north-south component of the El Centro ground motion; the particular version used is from Chopra (1995). Implementation details are presented next for selected systems and final results for all systems in Table 2.

The procedure is implemented for System 5 (Table 1).

1. Implementation of Step 1 gives the 5%-damped elastic demand diagram and the capacity diagram in Fig. 5a.

2. Assume $D_i = D(1.0,5\%) = 11.27$ cm.

3. $\mu = 11.27 \div 2.562 = 4.40$.

4. $\zeta_{eq} = 0.637 \times (4.40 - 1) \div 4.40 = 0.49$; instead use the maximum allowable value 0.45. For $\zeta_{eq} = 0.45$ and Type A systems (Fig. 4), $\kappa = 0.77$ and $\hat{\zeta}_{eq} = \zeta + \kappa \zeta_{eq} = 0.05 + 0.77 \times 0.45 = 0.397$.

5. The elastic demand diagram for 39.7% damping intersects the capacity diagram at $D_j = 3.725$ cm (Fig. 5a).

6. $100 \times (D_j - D_i) \div D_j = 100 \times (3.725 - 11.27) \div 3.725 = -202.6\%$ > 5% tolerance. Set $D_i = 3.725$ cm and repeat Steps 3 to 6.

For the second iteration, $D_i = 3.725$ cm, $\mu = 3.725 \div 2.562 = 1.45$, $\zeta_{eq} = 0.637 \times (1.45 - 1) \div 1.45 = 0.198$, κ= 0.98, and $\hat{\zeta}_{eq} = 0.243$. The intersection point $D_j = 5.654$ cm and the difference between D_i and D_j = 34.1% which is greater than the 5% tolerance. Therefore, additional iterations are required; results of these iterations are summarized in Table 3. Error becomes less than the 5% tolerance at the end of sixth iteration and the procedure could have been stopped there. However, the procedure was continued until the error became practically equal to zero. The deformation demand at the end of the iteration process, $D_j = 4.458$ cm. Determined by response history analysis (RHA) of the inelastic system, $D_{exact} = 10.16$ cm and the error = $100 \times (4.458 - 10.16) \div 10.16 = -56.1\%$.

Fig. 5b shows the convergence behavior of the ATC-40 Procedure A for System 5. Observe that this iterative procedure converges to a deformation much smaller than the exact value. Thus convergence here is deceptive because it can leave the erroneous impression that the calculated deformation is accurate. In contrast, a rational iterative procedure should lead to the exact result after a sufficient number of iterations.

The procedure is next implemented for System 6 (Table 1).

1. Implementation of Step 1 gives the 5%-damped elastic demand diagram and capacity diagram in Fig. 6a.

2. Assume $D_i = D(1.0,5\%) = 11.27$ cm.

3. $\mu = 11.27 \div 4.302 = 2.62$.

4. $\zeta_{eq} = 0.637 \times (2.62 - 1) \div 2.62 = 0.39$. For $\zeta_{eq} = 0.39$ and Type A systems (Fig. 4), $\kappa = 0.82$ and $\hat{\zeta}_{eq} = \zeta + \kappa \zeta_{eq} = 0.05 + 0.82 \times 0.39 = 0.371$.

5. The elastic demand diagram for 37.1% damping intersects the capacity diagram at $D_j = 3.538$ cm (Fig. 6a).

6. $100 \times (D_j - D_i) \div D_j = 100 \times (3.538 - 11.27) \div 3.538 = -218.6\%$ > 5% tolerance. Set $D_i = 3.538$ cm and repeat Steps 3 to 6.

The results for subsequent iterations, summarized in Table 4, indicate that the procedure fails to converge for this example. In the first iteration, the 37.1%-damped elastic demand diagram intersects the capacity diagram in its linear-elastic region (Fig. 6a). In subsequent iterations, the intersection point alternates between 11.73 cm and 3.515 cm (Table 4 and Fig. 6b). In order to examine if the procedure would converge with a new starting point, the procedure was restarted with $D_i = 5$ cm at iteration number 7. However, the procedure diverges very quickly as shown by iterations 7 to 15 (Table 4 and Fig. 6b), ending in an alternating pattern.

Table 1. Properties of example systems and their response to El Centro (1940) ground motion.

System Properties				System Response	
System	T_n (s)	$f_y \div w$	u_y (cm)	μ	D_{exact} (cm)
1	0.5	0.1257	0.7801	6	4.654
2		0.1783	1.106	4	4.402
3		0.3411	2.117	2	4.210
4	1	0.07141	1.773	6	10.55
5		0.1032	2.562	4	10.16
6		0.1733	4.302	2	8.533

Table 2. Results from ATC-40 Procedure A analysis of six systems for El Centro (1940) ground motion.

System	Converged (?)	D_{approx} (cm)	D_{exact} (cm)	Error (%)
1	Yes	3.534	4.654	-24.1
2	Yes	3.072	4.402	-30.2
3	No	--	4.210	--
4	Yes	7.912	10.55	-25.0
5	Yes	4.458	10.16	-56.1
6	No	--	8.533	--

Table 3. Detailed results from ATC-40 Procedure A analysis of System 5 for El Centro (1940) ground motion.

Iteration No.	D_i	A_i	$\hat{\zeta}_{eq}$	D_j	A_j	Difference (%)
1	11.272	0.1032	0.3965	3.7252	0.1032	-202.6
2	3.7252	0.1032	0.2432	5.6537	0.1032	34.1
3	5.6537	0.1032	0.3466	4.0832	0.1032	-38.5
4	4.0832	0.1032	0.2732	4.7214	0.1032	13.5
5	4.7214	0.1032	0.3114	4.3523	0.1032	-8.5
6	4.3523	0.1032	0.2912	4.5002	0.1032	3.3
7	4.5002	0.1032	0.2999	4.4425	0.1032	-1.3
8	4.4425	0.1032	0.2966	4.4639	0.1032	0.5
9	4.4639	0.1032	0.2978	4.4561	0.1032	-0.2
10	4.4561	0.1032	0.2974	4.4589	0.1032	0.1
11	4.4589	0.1032	0.2975	4.4579	0.1032	0

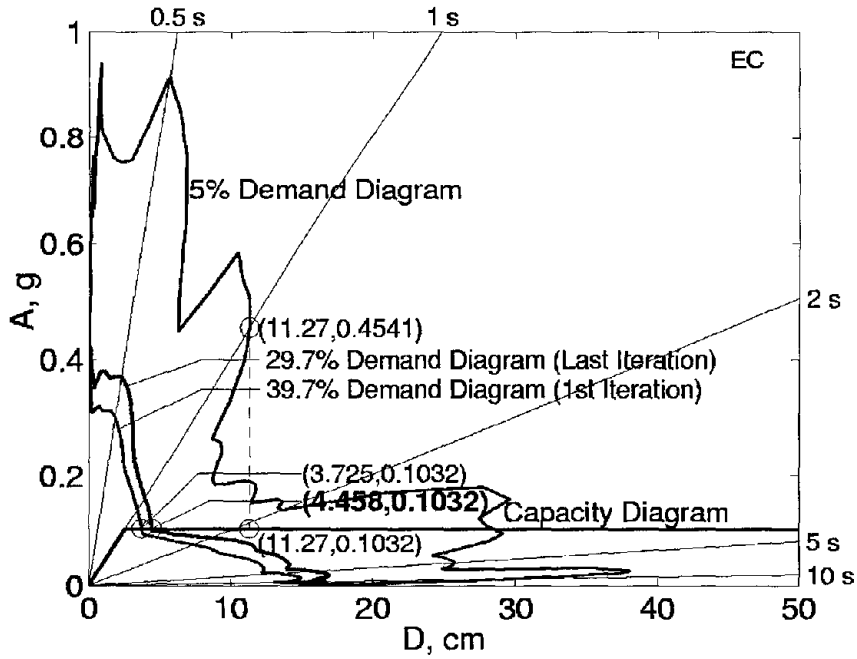

(a)

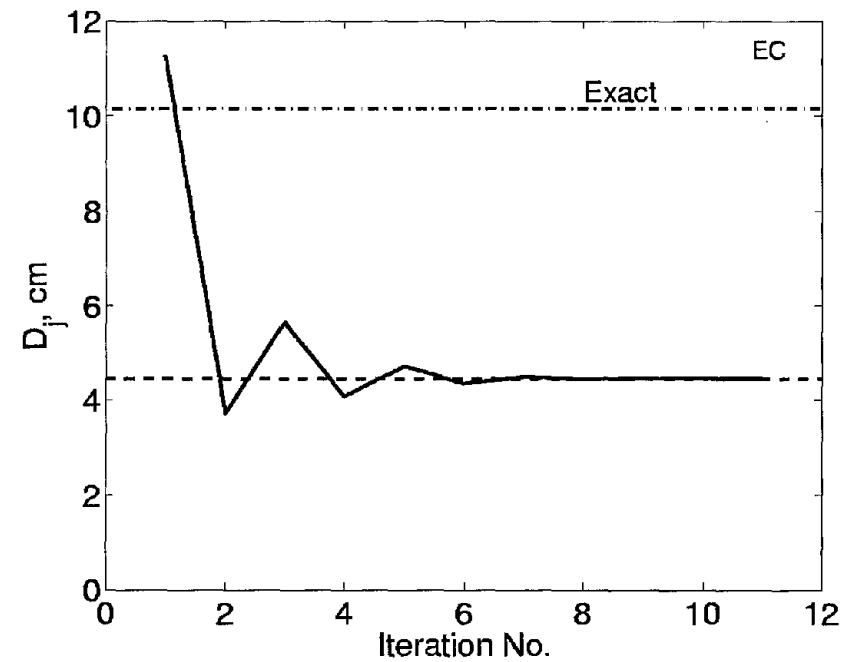

(b)

Figure 5. Application of ATC-40 Procedure A to System 5 for El Centro (1940) ground motion: (a) iterative procedure, and (b) convergence behavior.

Table 4. Detailed results from ATC-40 Procedure A analysis System 6 for El Centro (1940) ground motion.

Iteration No.	D_i	A_i	$\hat{\xi}_{eq}$	D_j	A_j	Difference (%)	Comments
1	11.272	0.1733	0.371	3.5376	0.14251	-218.6	Start with elastic response
2	3.5376	0.1733	0.05	11.726	0.1733	69.8	
3	11.726	0.1733	0.3756	3.5146	0.14158	-233.6	
4	3.5146	0.1733	0.05	11.726	0.1733	70	
5	11.726	0.1733	0.3756	3.5146	0.14158	-233.6	
6	3.5146	0.1733	0.05	11.726	0.1733	70	Indefinite oscillation
7	5	0.1733	0.1389	5.6491	0.1733	11.5	Iteration restarted
8	5.6491	0.1733	0.2019	4.856	0.1733	-16.3	
9	4.856	0.1733	0.1227	6.1903	0.1733	21.6	
10	6.1903	0.1733	0.2394	4.2884	0.17276	-44.3	
11	4.2884	0.1733	0.05	11.726	0.1733	63.4	
12	11.726	0.1733	0.3756	3.5146	0.14158	-233.6	
13	3.5146	0.1733	0.05	11.726	0.1733	70	
14	11.726	0.1733	0.3756	3.5146	0.14158	-233.6	
15	3.5146	0.1733	0.05	11.726	0.1733	70	Failure to converge
16	5.3	0.1733	0.17	5.3711	0.1733	1.3	Iteration restarted
17	5.3711	0.1733	0.1768	5.2752	0.1733	-1.8	
18	5.2752	0.1733	0.1675	5.4011	0.1733	2.3	
19	5.4011	0.1733	0.1796	5.2299	0.1733	-3.3	
20	5.2299	0.1733	0.163	5.4519	0.1733	4.1	
21	5.4519	0.1733	0.1844	5.1522	0.1733	-5.8	
22	5.1522	0.1733	0.1551	5.5307	0.1733	6.8	
23	5.5307	0.1733	0.1915	5.0337	0.1733	-9.9	
24	5.0337	0.1733	0.1426	5.6263	0.1733	10.5	
25	5.6263	0.1733	0.1999	4.8902	0.1733	-15.1	
26	4.8902	0.1733	0.1266	6.0294	0.1733	18.9	
27	6.0294	0.1733	0.2296	4.3819	0.1733	-37.6	
28	4.3819	0.1733	0.0616	11.077	0.1733	60.4	
29	11.077	0.1733	0.3688	3.5484	0.14294	-212.2	
30	3.5484	0.1733	0.05	11.726	0.1733	69.7	
31	11.726	0.1733	0.3756	3.5146	0.14158	-233.6	
32	3.5146	0.1733	0.05	11.726	0.1733	70	
33	11.726	0.1733	0.3756	3.5146	0.14158	-233.6	Slow divergence

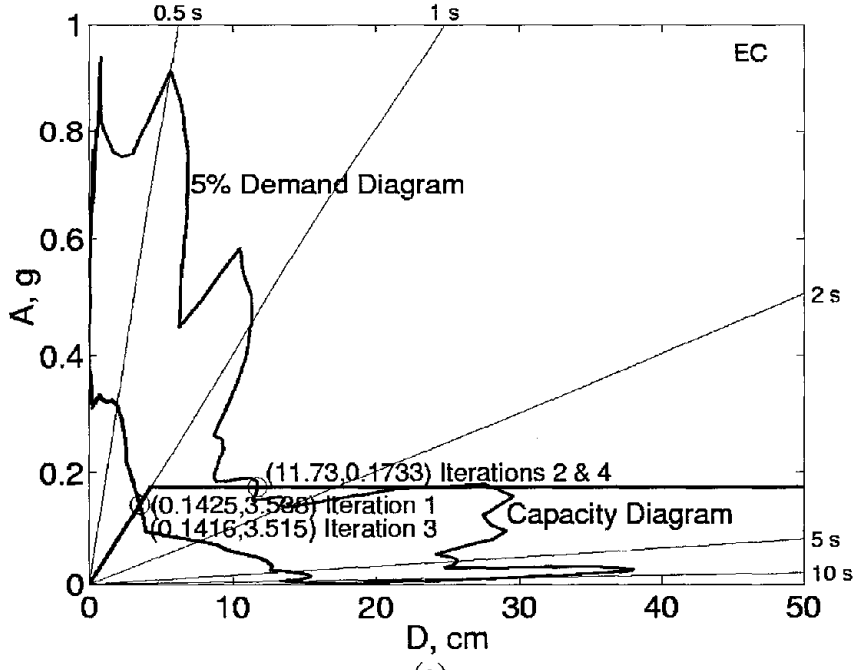

(a)

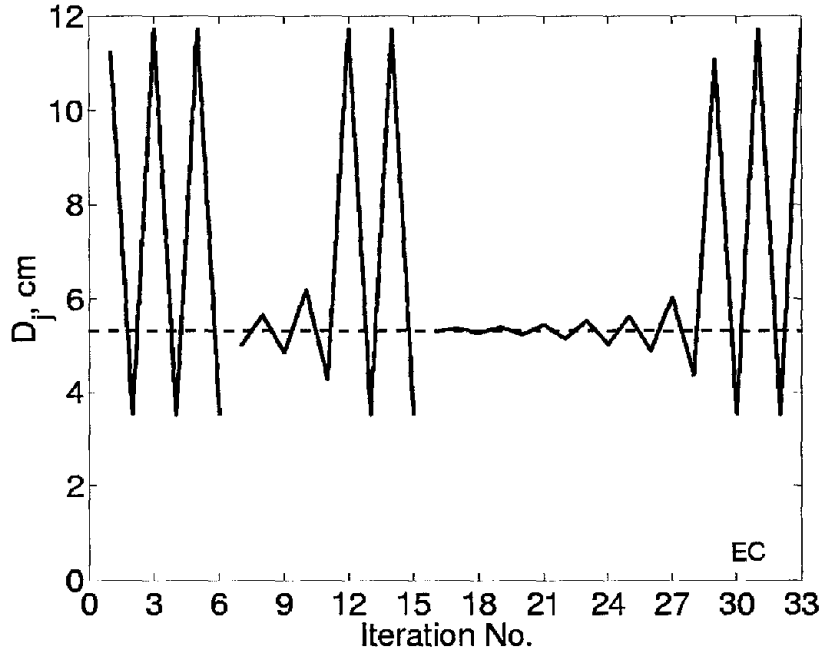

(b)

Figure 6. Application of ATC-40 Procedure A to System 6 for El Centro (1940) ground motion: (a) iterative procedure, and (b) convergence behavior.

Examples: Design Spectrum

The ATC-40 Procedure A is next implemented to analyze systems with the excitation specified by a design spectrum. For illustration we have selected the design spectrum of Fig. 7, which is the median-plus-one-standard-deviation spectrum constructed by the procedures of Newmark and Hall (1982), as described in Chopra (1995; Section 6.9). The systems analyzed have the same T_n as those considered previously but their yield strengths for the selected μ values were determined from the design spectrum (Table 5). Implementation details are presented next for selected systems and the final results for all systems in Table 6.

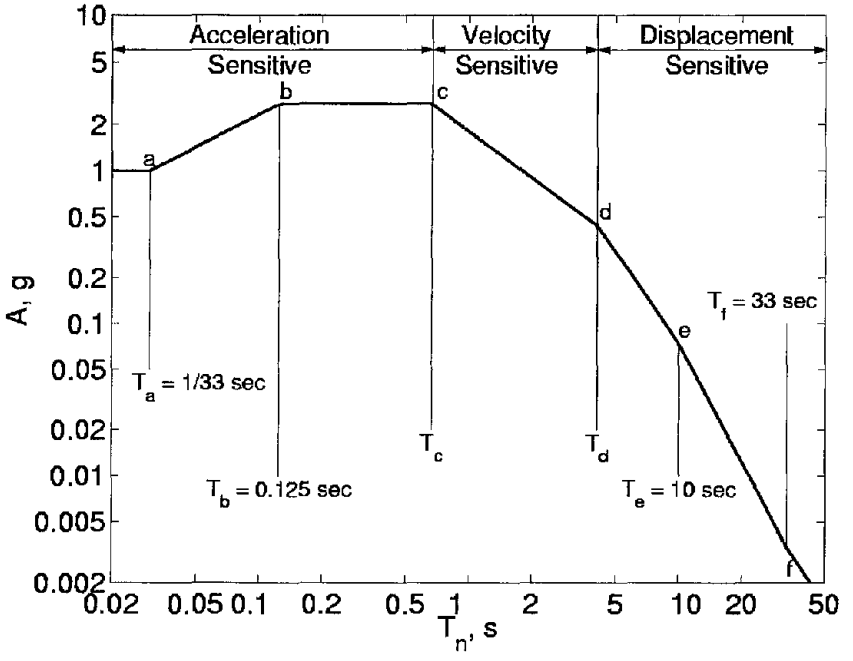

Figure 7. Newmark-Hall elastic design spectrum.

The procedure is implemented for System 5 (Table 5).

1. Implementation of Step 1 gives the 5%-damped elastic demand diagram and capacity diagram in Fig. 8a.
2. Assume $D_i = D(1.0,5\%) = 44.64$ cm.
3. $\mu = 44.64 \div 11.16 = 4$.
4. $\zeta_{eq} = 0.637 \times (4.0 - 1) \div 4.0 = 0.48$; instead use the maximum allowable value 0.45. For $\zeta_{eq} = 0.45$ and Type A systems (Fig. 4), $\kappa = 0.77$ and $\hat{\zeta}_{eq} = \zeta + \kappa \zeta_{eq} = 0.05 + 0.77 \times 0.45 = 0.397$

5. The elastic demand diagram for 39.7% damping intersects the capacity diagram at $D_j = 28.18$ cm (Fig. 8a).

6. $100 \times (D_j - D_i) \div D_j = 100 \times (28.18 - 44.64) \div 28.18 = -58.4\% > 5\%$ tolerance. Set D_i = 28.18 cm and repeat Steps 3 to 6.

For the second iteration, $D_i = 28.18$ cm, $\mu = 28.18 \div 11.16 = 2.52$, $\zeta_{eq} = 0.637 \times (2.52 - 1) \div 2.52 = 0.38$, κ= 0.84, and $\hat{\zeta}_{eq} = 0.37$. The intersection point $D_j = 31.55$ cm and the difference between D_i and D_j = 10.7% which is greater than the 5% tolerance. Therefore, additional iterations are required; results of these iterations are summarized in Table 7. The error becomes less than the 5% tolerance at the end of fourth iteration and the procedure could have been stopped there. However, the procedure was continued till the error became practically equal to zero. The deformation demand at the end of the iteration process is $D_j = 30.44$ cm.

Determined directly from the inelastic design spectrum, constructed by the procedures of Newmark and Hall (1982), as described in Chopra (1995, Section 7.10), the "reference" value of deformation is $D_{spectrum} = 44.64$ cm and the discrepancy = $100 \times (30.44 - 44.64) \div 44.64$ = -31.8%.

Fig. 8b shows the convergence behavior of the ATC-40 Procedure A for System 5. Observe that the iterative procedure converges to a deformation value much smaller than the "reference" value.

The procedure is next implemented for System 6 (Table 5).

1. Implementation of Step 1 gives the 5%-damped elastic demand diagram and capacity diagram in Fig. 9a.

2. Assume $D_i = D(0.5,5\%) = 44.64$ cm.

3. $\mu = 44.64 \div 22.32 = 2.0$.

4. $\zeta_{eq} = 0.637 \times (2.0 - 1) \div 2.0 = 0.32$. For $\zeta_{eq} = 0.32$ and Type A systems (Fig. 4), $\kappa = 0.87$ and $\hat{\zeta}_{eq} = \zeta + \kappa \zeta_{eq} = 0.05 + 0.87 \times 0.32 = 0.33$.

5. The elastic demand diagram for 33% damping intersects the capacity diagram at $D_j = 18.56$ cm (Fig. 9a).

6. $100 \times (D_j - D_i) \div D_j = 100 \times (18.56 - 44.64) \div 18.56 = -140.6\% > 5\%$ tolerance. Set $D_i = 18.56$ cm and repeat Steps 3 to 6.

The results for subsequent iterations, summarized in Table 8, indicate that the procedure fails to converge for this example. In the first iteration, the 33%-damped elastic demand diagram intersects the capacity diagram in its linear-elastic region (Fig. 9a). In subsequent iterations, the intersection point alternates between 13.72 cm and 89.28 cm (Table 8 and Fig. 9b). In order to examine if the procedure would converge with a new starting point, the procedure was restarted with $D_i = 28$ cm at iteration number 6. However, the procedure diverges very quickly as shown by iterations 6 to 11 (Table 8 and Fig. 9b), ending in an alternating pattern.

Table 5. Properties of example systems and their deformations from inelastic design spectrum.

System Properties				System Response	
System	T_n (s)	$f_y \div w$	u_y (cm)	μ	$D_{spectrum}$ (cm)
1	0.5	0.5995	3.7202	6	22.32
2		0.8992	5.5803	4	22.32
3		1.5624	9.6962	2	19.39
4	1	0.2997	7.4403	6	44.64
5		0.4496	11.160	4	44.64
6		0.8992	22.321	2	44.64

Table 6. Results from ATC-40 Procedure A analysis of six systems for design spectrum.

System	Converged (?)	D_{approx} (cm)	$D_{spectrum}$ (cm)	Discrepancy (%)
1	No	--	22.32	--
2	No	--	22.32	--
3	No	--	19.39	--
4	No	--	44.64	--
5	Yes	30.44	44.64	-31.8
6	Yes	42.28	44.64	-5.3

Table 7. Detailed results ATC-40 Procedure A analysis of System 5 for design spectrum.

Iteration No.	D_i	A_i	$\hat{\zeta}_{eq}$	D_j	A_j	Difference (%)
1	44.64	0.4496	0.3965	28.18	0.4496	-58.4
2	28.18	0.4496	0.3664	31.55	0.4496	10.7
3	31.54	0.4496	0.3796	30.01	0.4496	-5.1
4	30.01	0.4496	0.3741	30.64	0.4496	2
5	30.64	0.4496	0.3764	30.37	0.4496	-0.9
6	30.36	0.4496	0.3754	30.48	0.4496	0.4
7	30.48	0.4496	0.3759	30.43	0.4496	-0.2
8	30.43	0.4496	0.3757	30.45	0.4496	0.1
9	30.45	0.4496	0.3757	30.44	0.4496	0

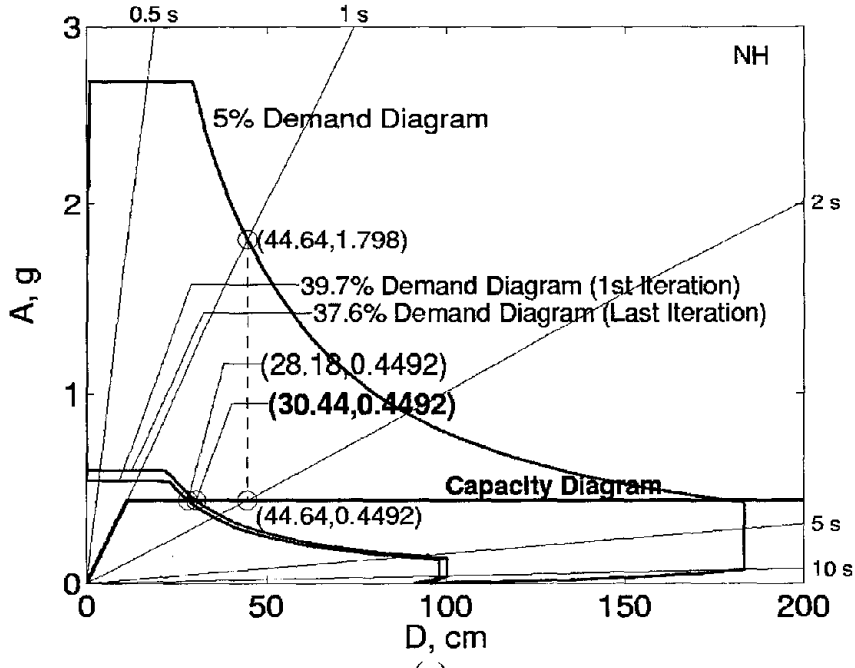

(a)

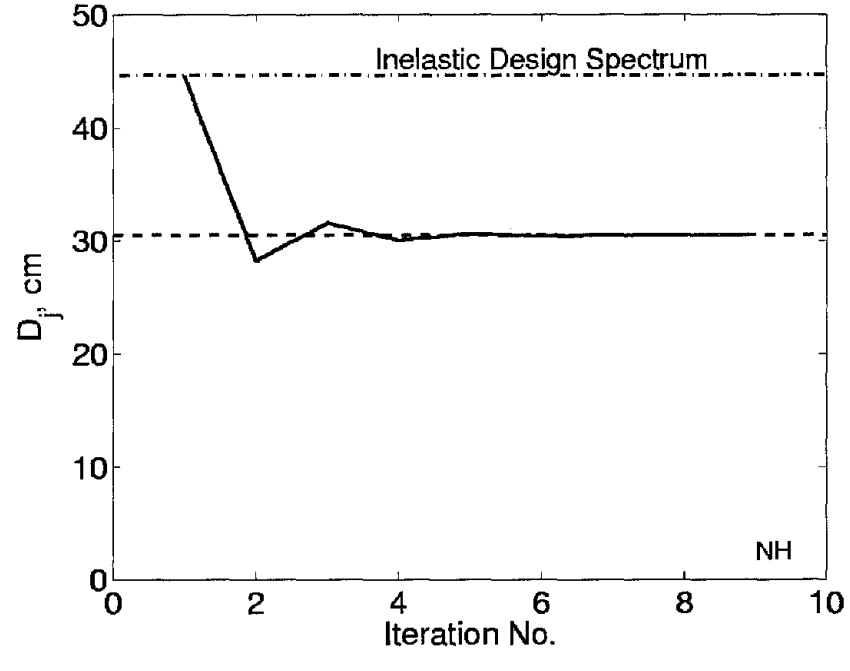

(b)

Figure 8. Application of ATC-40 Procedure A to Example 5 for elastic design spectrum: (a) iterative procedure, and (b) convergence behavior.

Table 8. Detailed results ATC-40 Procedure A analysis of System 6 for design spectrum.

Iteration No.	D_i	A_i	$\hat{\xi}_{eq}$	D_j	A_j	Difference (%)	Comments
1	44.64	0.8992	0.3288	18.56	0.7475	-140.6	Start with elastic response
2	18.56	0.8992	0.0500	89.28	0.8992	79.2	
3	89.28	0.8992	0.3965	13.72	0.5527	-550.7	
4	13.72	0.8992	0.0500	89.28	0.8992	84.6	
5	89.28	0.8992	0.3965	13.72	0.5527	-550.7	Indefinite oscillation
6	28.00	0.8992	0.1792	35.27	0.8992	20.6	Iteration restarted
7	35.27	0.8992	0.2705	23.10	0.8992	-52.7	
8	23.10	0.8992	0.0715	71.67	0.8992	67.8	
9	71.67	0.8992	0.3917	14.03	0.5653	-410.7	
10	14.03	0.8992	0.0500	89.28	0.8992	84.3	
11	89.28	0.8992	0.3965	13.72	0.5527	-550.7	Indefinite oscillation
12	29.00	0.8992	0.1967	32.29	0.8992	10.2	Iteration restarted
13	32.29	0.8992	0.2413	26.23	0.8992	-23.1	
14	26.23	0.8992	0.1449	42.56	0.8992	38.4	
15	42.56	0.8992	0.3189	19.34	0.7791	-120.1	
16	19.34	0.8992	0.0500	89.28	0.8992	78.3	
17	89.28	0.8992	0.3965	13.72	0.5527	-550.7	
18	13.72	0.8992	0.0500	89.28	0.8992	84.6	
19	89.28	0.8992	0.3965	13.72	0.5527	-550.7	Slow divergence

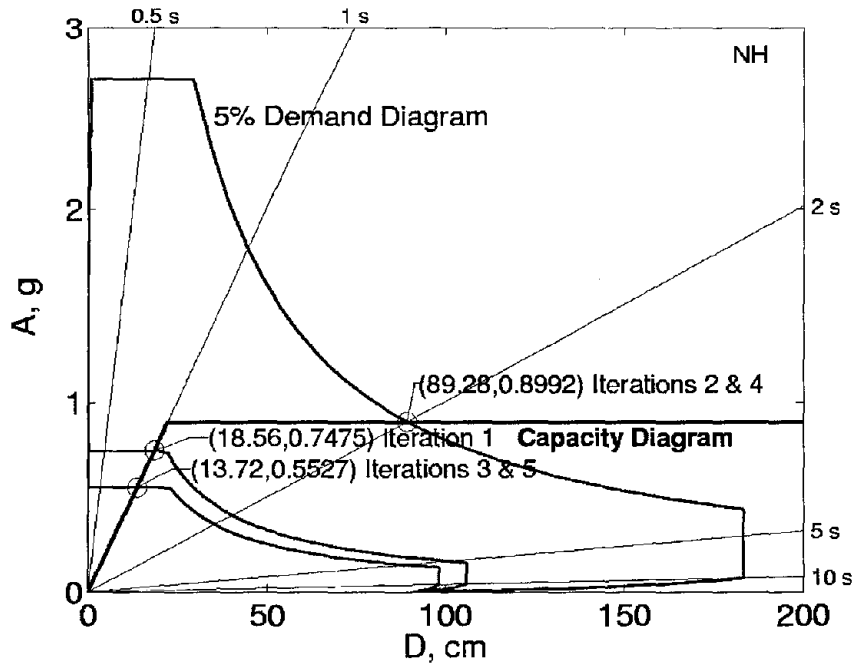

(a)

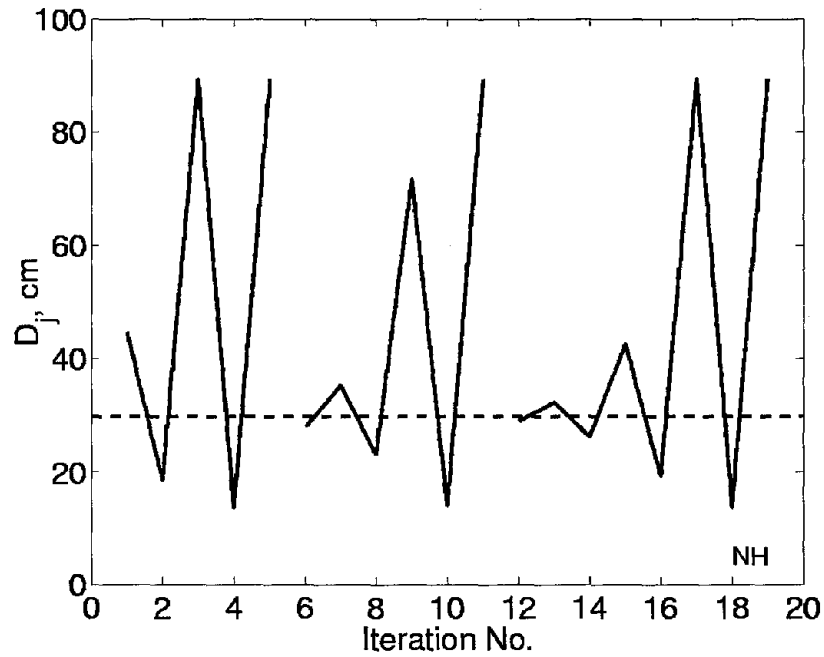

(b)

Figure 9. Application of ATC-40 Procedure A to System 6 for elastic design spectrum: (a) iterative procedure, and (b) convergence behavior.

PROCEDURE B

This procedure in the ATC-40 report is described herein as a sequence of steps:

1. Plot the capacity diagram.
2. Estimate the peak deformation demand D_i. Initially assume $D_i = D(T_n, \zeta = 5\%)$.
3. Compute ductility $\mu = D_i \div u_y$.
4. Compute equivalent period T_{eq} and damping ratio $\hat{\xi}_{eq}$ from Eqs. (2) and (7), respectively.
5. Compute the peak deformation $D(T_{eq}, \hat{\xi}_{eq})$ and peak pseudo-acceleration $A(T_{eq}, \hat{\xi}_{eq})$ of an elastic SDF system with vibration properties T_{eq} and $\hat{\xi}_{eq}$.
6. Plot the point with coordinates $D(T_{eq}, \hat{\xi}_{eq})$ and $A(T_{eq}, \hat{\xi}_{eq})$.
7. Check if the curve generated by connecting the point plotted in Step 6 to previously determined, similar points intersects the capacity diagram. If not, repeat Steps 3-7 with a new value of D_i; otherwise go to Step 8.
8. The earthquake-induced deformation demand is given by the D-value at the intersection point.

Examples: Specified Ground Motion

Procedure B is implemented for the Systems 1 to 6 (Table 1). The final results are summarized in Table 9; details are presented next. For a number of assumed values of μ (or D), pairs of values $D(T_{eq}, \hat{\xi}_{eq})$ and $A(T_{eq}, \hat{\xi}_{eq})$ are generated (Tables 10 and 11). These pairs are plotted to obtain the curve *A-B* in Fig. 10, wherein capacity diagrams for three systems are shown together with the 5%-damped linear elastic demand diagram; the latter need not be plotted. The intersection point between the curve *A-B* and the capacity diagram of a system gives its deformation demand: $D = 3.536$ cm, $D = 3.075$ cm, and $D = 3.284$ cm for Systems 1 to 3, respectively (Fig. 10a); and $D = 7.922$ cm, $D = 4.454$ cm, and $D = 5.318$ cm for Systems 4 to 6, respectively (Fig. 10b). In contrast, the exact deformations computed by RHA of the inelastic systems are 4.654 cm, 4.402 cm, and 4.210 cm for Systems 1 to 3; and 10.55 cm, 10.16 cm, and 8.533 cm for Systems 4 to 6, indicating that the error in the approximate procedure ranges from –22% to –56.2%. Observe that the curve *A-B* provides the information to determine the deformation demand in several systems with the same T_n values but different yield strengths.

Procedure B always gives a unique estimate of the deformation, whereas, as noted earlier, the iterative Procedure A may not always converge. If it does converge, the two procedures give the same value of deformation (within round-off and interpolation errors) in the examples solved.

Table 9. Results from ATC-40 Procedure B analysis of six systems for El Centro ground motion.

System	D_{approx} (cm)	D_{exact} (cm)	Discrepancy (%)
1	3.536	4.654	-24.0
2	3.075	4.402	-30.1
3	3.284	4.210	-22.0
4	7.922	10.55	-24.9
5	4.453	10.16	-56.2
6	5.318	8.533	-37.7

Table 10. Detailed results from ATC-40 Procedure B analysis of Systems 1 to 3 for El Centro (1940) ground motion.

μ	T_{eq}	$\hat{\zeta}_{eq}$	D	A
1	0.5	0.05	5.6846	0.91599
1.1	0.5244	0.1079	4.411	0.64616
1.2	0.5477	0.1562	4.0093	0.53837
1.3	0.5701	0.197	3.7297	0.46229
1.4	0.5916	0.2292	3.5032	0.40321
1.5	0.6124	0.2539	3.3449	0.35933
1.55	0.6225	0.2646	3.2859	0.3416
1.5515	**0.6228**	**0.2649**	**3.2842**	**0.3411**
1.5531	0.6228	0.2649	3.2854	0.34085
1.6	0.6325	0.2743	3.228	0.3251
1.7	0.6519	0.2914	3.1162	0.29537
1.8	0.6708	0.3058	3.0093	0.26939
1.9	0.6892	0.3182	2.9207	0.2477
2	0.7071	0.3288	2.8739	0.23155
2.1	0.7246	0.338	2.898	0.22237
2.2	0.7416	0.3461	2.9204	0.2139
2.3	0.7583	0.3532	2.9412	0.20606
2.4	0.7746	0.3595	2.9605	0.19877
2.5	0.7906	0.365	2.9929	0.19291
2.6	0.8062	0.37	3.024	0.18742
2.7	0.8216	0.3745	3.0531	0.18221
2.7787	**0.8335**	**0.3778**	**3.0747**	**0.1783**
2.8	0.8367	0.3786	3.0804	0.17727
2.9	0.8515	0.3823	3.1058	0.17257
3	0.866	0.3856	3.1295	0.16809
3.1	0.8803	0.3887	3.1517	0.16382
3.2	0.8944	0.3914	3.1723	0.15974
3.3	0.9083	0.394	3.1992	0.15621
3.4	0.922	0.3964	3.2273	0.15295
3.5	0.9354	0.3965	3.2632	0.15023
3.6	0.9487	0.3965	3.2973	0.14759
3.7	0.9618	0.3965	3.3293	0.14499
3.8	0.9747	0.3965	3.359	0.14244
3.9	0.9874	0.3965	3.3868	0.13993
4	1	0.3965	3.4126	0.13747
4.1	1.0124	0.3965	3.4366	0.13506
4.2	1.0247	0.3965	3.4588	0.1327
4.3	1.0368	0.3965	3.4792	0.13038
4.4	1.0488	0.3965	3.5023	0.12826
4.5	1.0607	0.3965	3.528	0.12633
4.525	1.0636	0.3965	3.5342	0.12585
4.533	**1.0645**	**0.3965**	**3.5362**	**0.1257**

Table 11. Detailed results from ATC-40 Procedure B analysis of Systems 4 to 6 for El Centro (1940) ground motion.

μ	T_{eq}	$\hat{\zeta}_{eq}$	D	A
1	1	0.05	11.272	0.45407
1.1	1.0488	0.1079	7.4536	0.27297
1.2	1.0954	0.1562	5.7066	0.19157
1.225	1.1068	0.167	5.4288	0.17852
1.2362	**1.1119**	**0.1717**	**5.3182**	**0.17330**
1.2375	1.1119	0.1717	5.3157	0.17304
1.3	1.1402	0.197	5.0373	0.15609
1.4	1.1832	0.2292	4.8741	0.14025
1.5	1.2247	0.2539	4.7401	0.12730
1.6	1.2649	0.2743	4.6154	0.11620
1.7	1.3038	0.2914	4.4969	0.10656
1.7384	**1.3185**	**0.2972**	**4.4535**	**0.1032**
1.8	1.3416	0.3058	4.3893	0.09823
1.9	1.3784	0.3182	4.5607	0.09670
2	1.4142	0.3288	4.7224	0.09512
2.1	1.4491	0.338	4.8831	0.09367
2.2	1.4832	0.3461	5.0397	0.09228
2.3	1.5166	0.3532	5.1901	0.09090
2.4	1.5492	0.3595	5.335	0.08955
2.5	1.5811	0.365	5.4748	0.08822
2.6	1.6125	0.37	5.6097	0.08692
2.7	1.6432	0.3745	5.7401	0.08564
2.8	1.6733	0.3786	5.8749	0.08452
2.9	1.7029	0.3823	6.0057	0.08343
3	1.7321	0.3856	6.1323	0.08234
3.1	1.7607	0.3887	6.2546	0.08128
3.2	1.7889	0.3914	6.3727	0.08023
3.3	1.8166	0.394	6.491	0.07924
3.4	1.8439	0.3964	6.6094	0.07831
3.5	1.8708	0.3965	6.742	0.07760
3.6	1.8974	0.3965	6.8714	0.07689
3.7	1.9235	0.3965	7.0005	0.07622
3.8	1.9494	0.3965	7.1297	0.07558
3.9	1.9748	0.3965	7.2543	0.07493
4	2	0.3965	7.3773	0.07430
4.1	2.0248	0.3965	7.501	0.07370
4.2	2.0494	0.3965	7.6197	0.07308
4.3	2.0736	0.3965	7.7332	0.07245
4.4	2.0976	0.3965	7.8442	0.07182
4.45	2.1095	0.3965	7.9008	0.07152
4.4688	**2.114**	**0.3965**	**7.9217**	**0.07141**

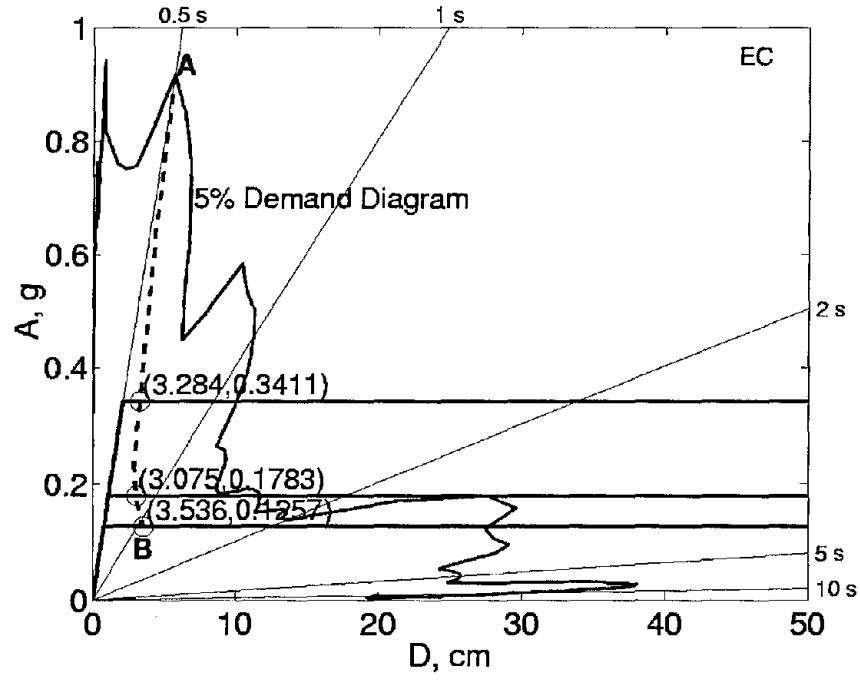

(a)

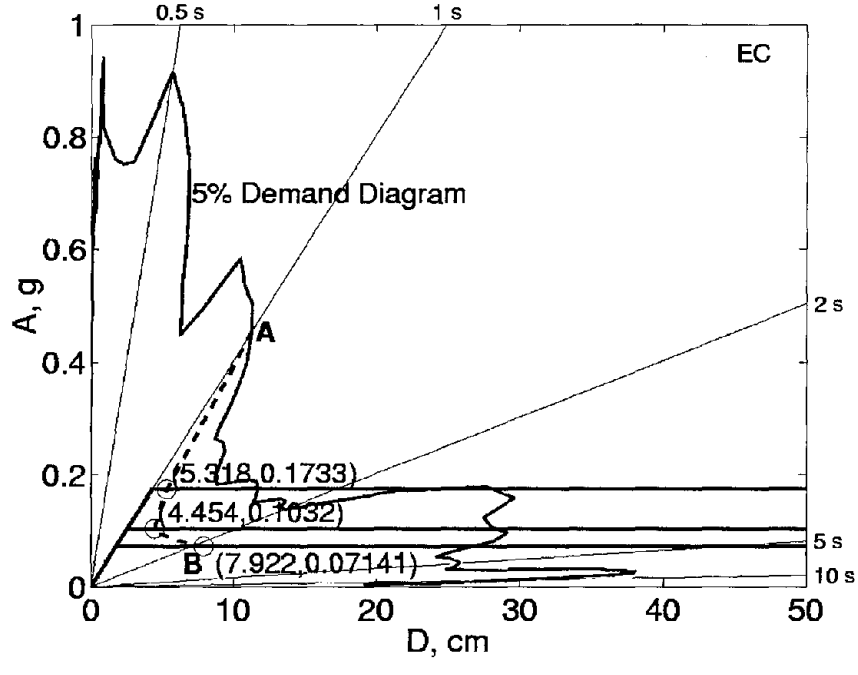

(b)

Figure 10. Application of ATC-40 Procedure B for El Centro (1940) ground motion: (a) Systems 1 to 3, and (b) Systems 4 to 6.

Examples: Design Spectrum

Procedure B is implemented for the Systems 1 to 6 (Table 5). The results from this procedure are summarized in Table 12 and illustrated in Fig. 11 where the estimated deformations are noted; intermediate results are available in Tables 13 and 14. These approximate values are compared in Table 12 against the values determined directly from the inelastic design spectrum constructed by the procedure of Newmark and Hall (1982), as described in Chopra (1995, Section 7.10); see Appendix B for details. Relative to these reference values, the discrepancy ranges from –5.2% to –58.6% for the systems considered.

Table 12. Results from ATC-40 Procedure B analysis of six systems for design spectrum.

System	D_{approx} (cm)	$D_{spectrum}$ (cm)	Discrepancy (%)
1	10.46	22.32	-53.1
2	9.245	22.32	-58.6
3	11.51	19.39	-40.6
4	42.27	44.64	-5.2
5	30.45	44.64	-31.7
6	29.84	44.64	-33.1

Table 13. Detailed results from ATC-40 Procedure B analysis of Systems 1 to 3 for design spectrum.

μ	T_{eq}	$\hat{\xi}_{eq}$	D	A
1	0.5	0.05	16.794	2.7062
1.1	0.5244	0.1079	13.012	1.9061
1.2	0.5477	0.1562	11.332	1.5217
1.1871	**0.5448**	**0.1504**	**11.51**	**1.5624**
1.3	0.5701	0.197	10.328	1.2802
1.4	0.5916	0.2292	9.7547	1.1227
1.5	0.6124	0.2539	9.4602	1.0163
1.6	0.6325	0.2743	9.2924	0.9358
1.6567	**0.6436**	**0.2843**	**9.2447**	**0.8992**
1.7	0.6519	0.2914	9.2107	0.8730
1.8	0.6708	0.3058	9.1906	0.8227
1.9	0.6892	0.3182	9.2164	0.7816
2	0.7071	0.3288	9.2776	0.7475
2.1	0.7246	0.338	9.3664	0.7187
2.2	0.7416	0.3461	9.4776	0.6942
2.3	0.7583	0.3532	9.607	0.6731
2.4	0.7746	0.3595	9.7515	0.6547
2.5	0.7906	0.365	9.9087	0.6387
2.6	0.8062	0.37	10.077	0.6245
2.7	0.8216	0.3745	10.254	0.6120
2.8	0.8367	0.3786	10.439	0.6008
2.8123	**0.8385**	**0.3791**	**10.463**	**0.5995**

Table 14. Detailed results from ATC-40 Procedure B analysis of Systems 4 to 6 for design spectrum.

μ	T_{eq}	$\hat{\zeta}_{eq}$	D	A
1	1	0.05	44.642	1.7984
1.2	1.0954	0.1562	32.69	1.0974
1.3519	**1.1627**	**0.2154**	**29.84**	**0.8892**
1.4	1.1832	0.2292	29.411	0.8463
1.6	1.2649	0.2743	28.488	0.7173
1.8	1.3416	0.3058	28.32	0.6338
2	1.4142	0.3288	28.521	0.5745
2.2	1.4832	0.3461	28.926	0.5297
2.4	1.5492	0.3595	29.448	0.4943
2.6	1.6125	0.37	30.042	0.4655
2.7283	**1.6517**	**0.3757**	**30.449**	**0.4496**
2.8	1.6733	0.3786	30.679	0.4414
3	1.7321	0.3856	31.343	0.4209
3.2	1.7889	0.3914	32.022	0.4031
3.4	1.8439	0.3964	32.708	0.3875
3.6	1.8974	0.3965	33.648	0.3765
3.8	1.9494	0.3965	34.57	0.3665
4	2	0.3965	35.468	0.3572
4.2	2.0494	0.3965	36.344	0.3486
4.4	2.0976	0.3965	37.199	0.3406
4.6	2.1448	0.3965	38.035	0.3331
4.8	2.1909	0.3965	38.853	0.3261
5	2.2361	0.3965	39.654	0.3195
5.2	2.2804	0.3965	40.44	0.3133
5.4	2.3238	0.3965	41.21	0.3074
5.6	2.3664	0.3965	41.966	0.3019
5.6822	**2.3837**	**0.3965**	**42.273**	**0.2997**

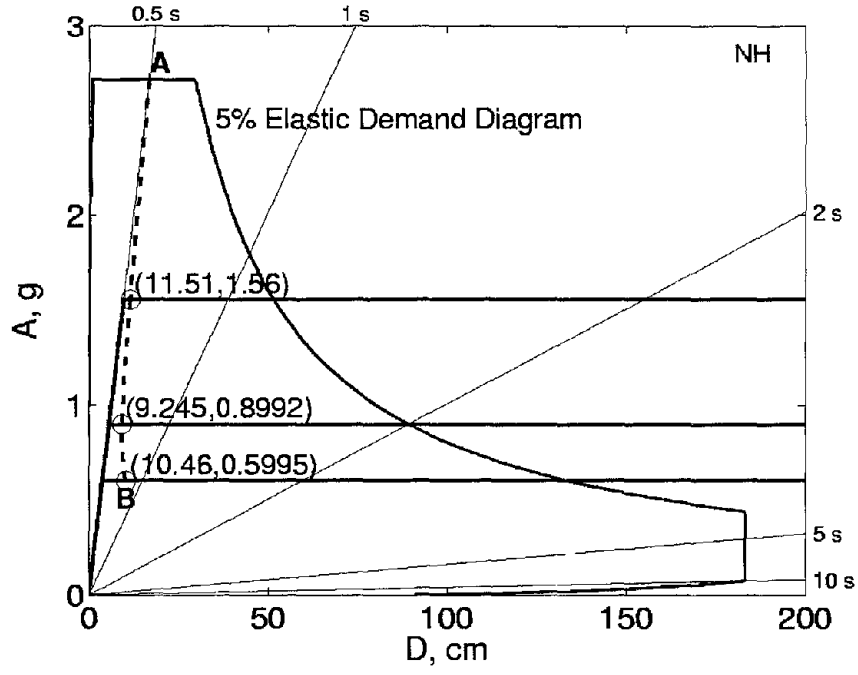

(a)

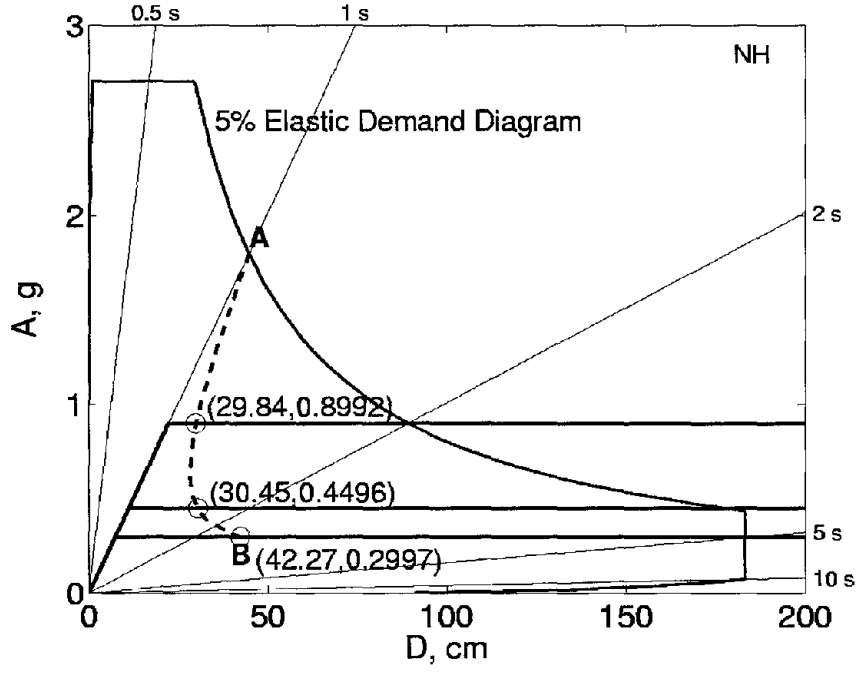

(b)

Figure 11. Application of ATC-40 Procedure B for elastic design spectrum: (a) Systems 1 to 3, and (b) Systems 4 to 6.

EVALUATION OF ATC-40 PROCEDURES

SPECIFIED GROUND MOTION

The ATC-40 Procedure B is implemented for a wide range of system parameters and excitations in two versions: (1) $\kappa = 1$, i.e., the equivalent viscous damping is given by Eqs. (4) and (5) based on well-established principles; and (2) κ is given by Fig. 4, a definition based primarily on judgment to account for different types of hysteretic behavior.

The yield strength of each elastoplastic system analyzed was chosen corresponding to an allowable ductility μ :

$$f_y = (A_y/g)w \tag{8}$$

where w is the weight of the system and A_y is the pseudo-acceleration corresponding to the allowable ductility and the vibration properties — natural period T_n and damping ratio ζ — of the system in its linear range of vibration. Recall that the ductility demand (computed by nonlinear response history analysis) imposed by the selected ground motion on systems defined in this manner will exactly equal the allowable ductility (Chopra, 1995; Section 19.1.1).

The peak deformation due to a selected ground motion, determined by the ATC-40 method, D_{approx}, is compared in Fig. 12 against the "exact" value, D_{exact}, determined by nonlinear RHA, and the percentage error in the approximate result is plotted in Fig. 13. These figures permit several observations. The approximate procedure is not especially accurate. It underestimates significantly the deformation for wide ranges of T_n values with errors approaching 50%, implying that the estimated deformation is only about half of the value determined by nonlinear RHA. The approximate method gives larger deformation for short period systems ($T_n < 0.1$ sec for $\mu = 2$ and $T_n < 0.4$ sec for $\mu = 6$) and the deformation does not approach zero as T_n goes to zero. This unreasonable discrepancy occurs because, for very short-period systems with small yield strength, the T_{eq} has to shift to the constant-V region of the spectrum before the capacity and demand diagrams can intersect (Appendix A). While inclusion of the damping modification factor κ increases the estimated displacement, the accuracy of the approximate results improves only marginally for the smaller values of μ. Therefore the κ factor is not attractive, especially because it is based primarily on judgement.

Shown in Fig. 14 are the errors in the ATC-40 method, with the κ factor included, for six different ground motions: (1) El Centro, S00E, 1940 Imperial Valley; (2) Corralitos, Chan-1, 90 deg, 1989 Loma Prieta; (3) Sylmar County Hospital Parking Lot, Chan-3, 360 deg, 1994 Northridge; (4) Pacoima Dam, N76W, 1971 San Fernando; (5) Lucerne Valley, S80W, 1992 Landers; and (6) SCT, S00E, 1985 Mexico City. Observe that, contrary to intuition, the error does not decrease consistently for smaller ductility. While the magnitude of the error and its variation with T_n depend on the excitation, the earlier observation that the error in the approximate method is significant is supported by results for several ground motions.

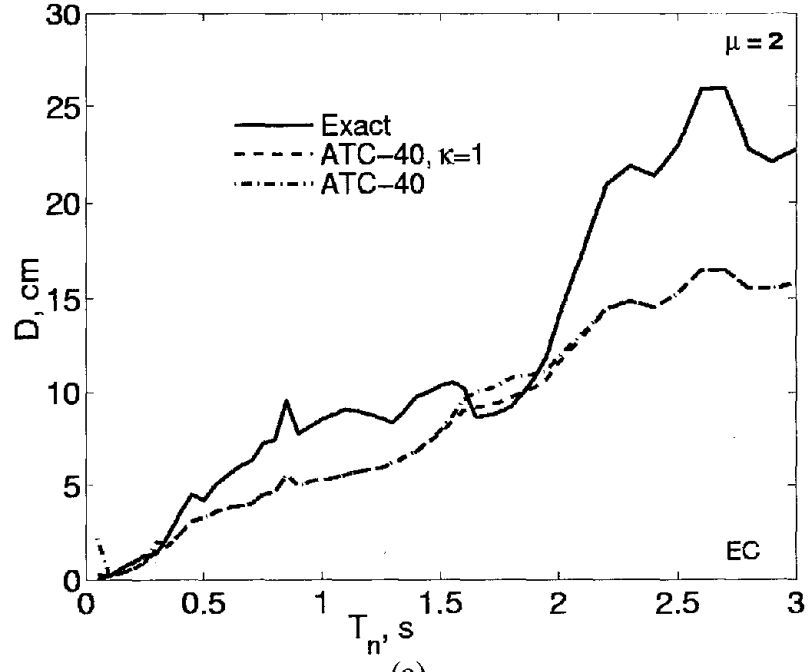

(a)

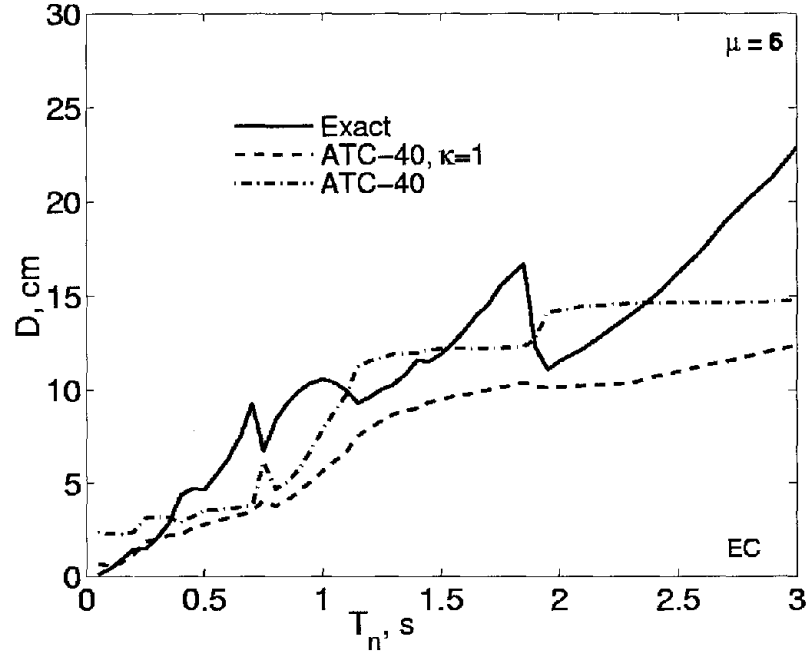

(b)

Figure 12. Comparison of deformations due to El Centro (1940) ground motion from approximate procedure and nonlinear response history analysis: (a) $\mu = 2$, and (b) $\mu = 6$.

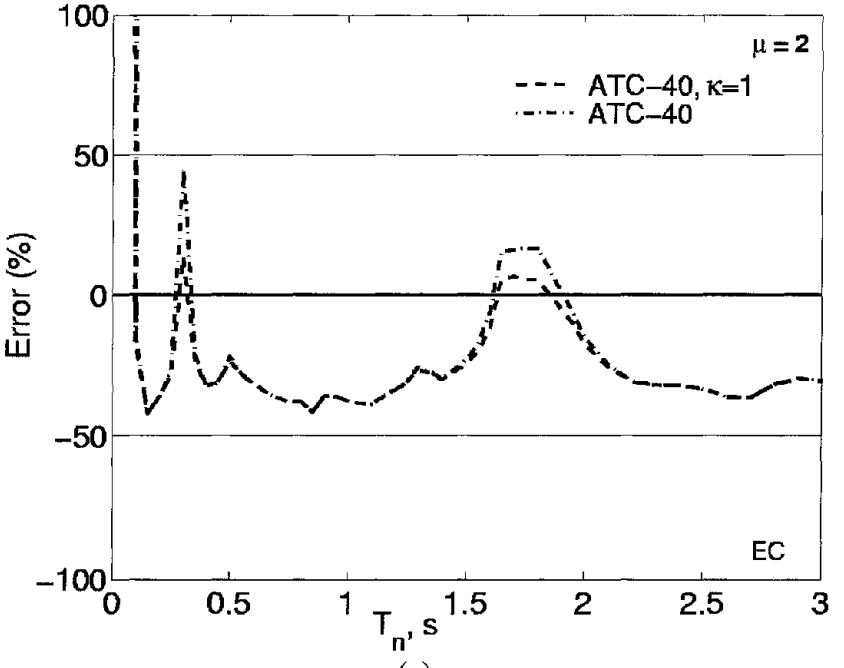

(a)

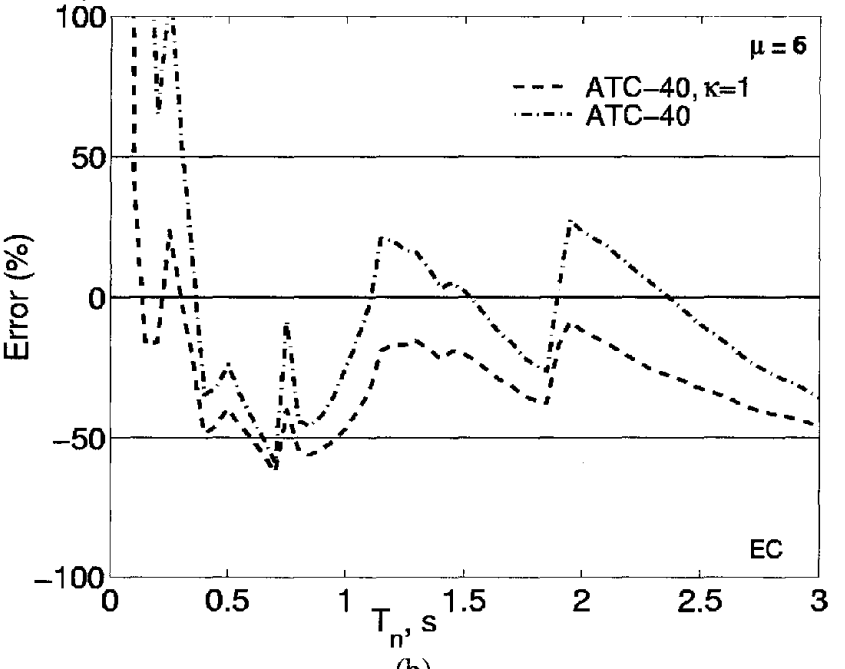

(b)

Figure 13. Error in deformations due to El Centro (1940) ground motion computed by approximate procedure: (a) μ = 2, and (b) μ = 6.

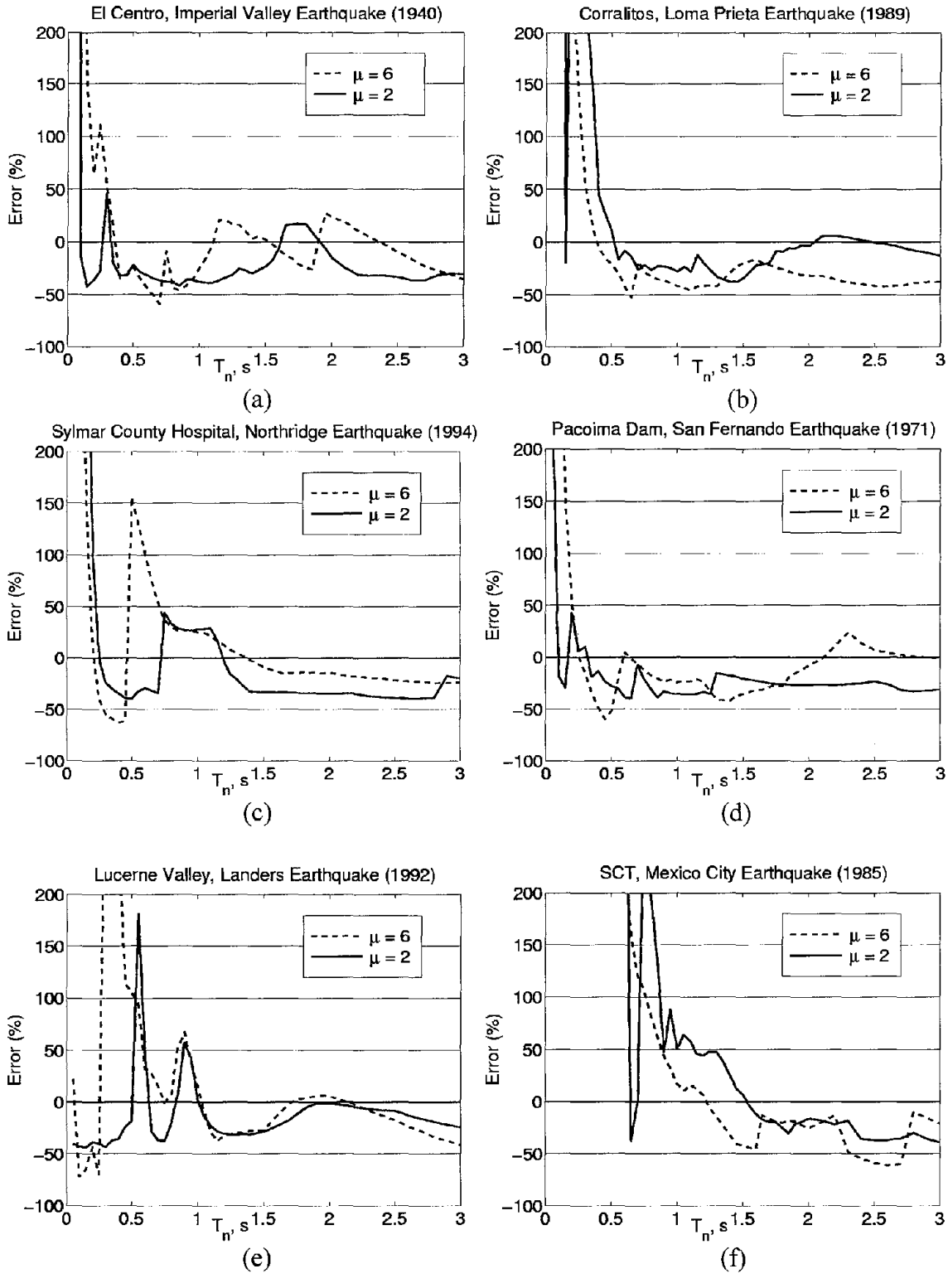

Figure 14. Error in deformations computed by approximate procedure for six ground motions.

DESIGN SPECTRUM

The ATC-40 Procedure B is implemented for a wide range of T_n and μ values with the excitation characterized by the elastic design spectrum of Fig. 7. The yield strength was defined by Eq. (8) with A_y determined from the inelastic design spectrum corresponding to the selected ductility factor. The resulting approximate values of deformations will be compared in this section with those determined directly from the design spectrum, as described next.

Given the properties T_n, ζ, f_y and α of the bilinear hysteretic system and the elastic design spectrum, the earthquake-induced deformation of the system can be determined directly from the design spectrum. The peak deformation D of this system is given by

$$D = \mu D_y \tag{9}$$

with the yield deformation defined by

$$D_y = \left(\frac{T_n}{2\pi}\right)^2 A_y \tag{10}$$

where A_y is the pseudo-acceleration related to the yield strength, f_y, by Eq. (8). Putting Eqs. (9) and (10) together gives

$$D = \mu\left(\frac{T_n}{2\pi}\right)^2 A_y \tag{11}$$

The yield strength reduction factor is given by

$$R_y = \frac{f_o}{f_y} = \frac{A}{A_y} \tag{12}$$

where

$$f_o = \left(\frac{A}{g}\right)w \tag{13}$$

is the minimum yield strength required for the structure to remain elastic; A is the pseudo-acceleration ordinate of the elastic design spectrum at (T_n, ζ). Substituting Eq. (12) in Eq. (11) gives

$$D = \mu\frac{1}{R_y}\left(\frac{T_n}{2\pi}\right)^2 A \tag{14}$$

Equation (14) provides a convenient way to determine the deformation of the inelastic system from the design spectrum. All that remains to be done is to determine μ for a given R_y; the latter is known from Eq. (12) for a structure with known f_y.

Presented in Fig. 15 are the deformations determined by Eq. 14 using three different $R_y - \mu - T_n$ equations: Newmark and Hall (1982); Krawinkler and Nassar (1992) for elastoplastic systems; and Vidic, Fajfar and Fischinger (1994) for bilinear systems. The equations describing these relationships are presented later in this report. Observe that the three recommendations lead to similar results except for $T_n < 0.3$ sec, indicating that the inelastic design spectrum is a reliable approach to estimate the earthquake-induced deformation of yielding systems.

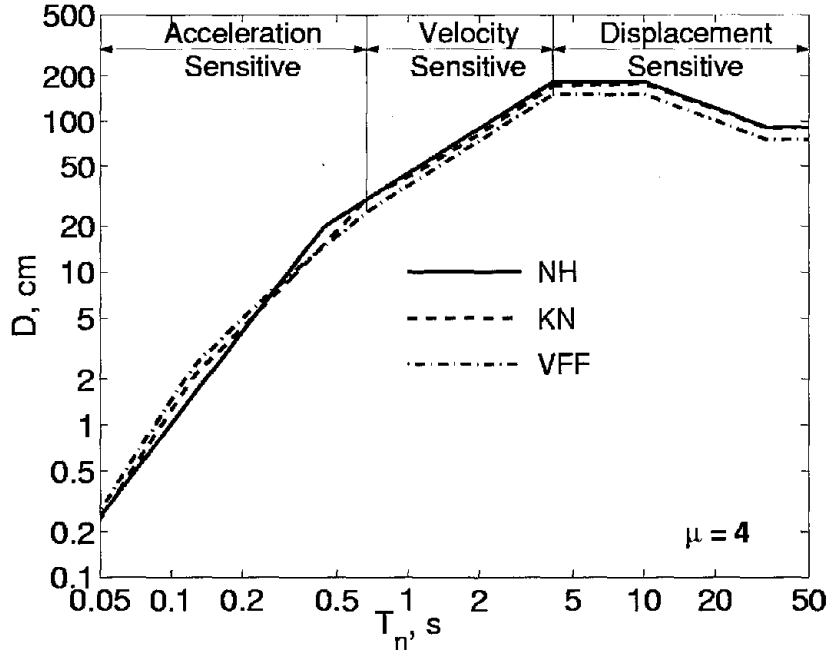

Figure 15. Deformation of inelastic systems (μ= 4) determined from inelastic design spectra using three $R_y - \mu - T_n$ equations: Newmark-Hall (NH), Krawinkler-Nassar (KN), and Vidic-Fajfar-Fischinger (VFF).

The deformation estimates by the ATC-40 method are compared in Fig. 16 with those from inelastic design spectra presented in Fig. 15. Relative to these "reference" values, the percentage discrepancy in the approximate result is plotted in Fig. 17. The results of Figs. 16 and 17 permit the following observations. The approximate procedure leads to significant discrepancy, except for very long periods ($T_n > T_f$ in Fig. 7). The magnitude of this discrepancy depends on the design ductility and the period region. In the acceleration-sensitive ($T_n < T_c$) and displacement-sensitive ($T_d < T_n < T_f$) regions (Fig. 7), the approximate procedure significantly underestimates the deformation; the discrepancy increases with increasing μ. In the velocity-sensitive ($T_c < T_n < T_d$) region, the ATC-40 procedure significantly underestimates the deformation for μ = 2 and 4, but overestimates it for μ = 8 and is coincidentally accurate for μ = 6.

In passing, note that the ATC-40 procedure is deficient relative to even the *elastic* design spectrum in the velocity-sensitive and displacement-sensitive regions ($T_n > T_c$). For T_n in these regions, the peak deformation of an inelastic system can be estimated from the elastic design spectrum, using the well-known equal-displacement rule (Veletsos and Newmark, 1960). However, the ATC-40 procedure requires analyses of several equivalent linear systems and still produces worse results.

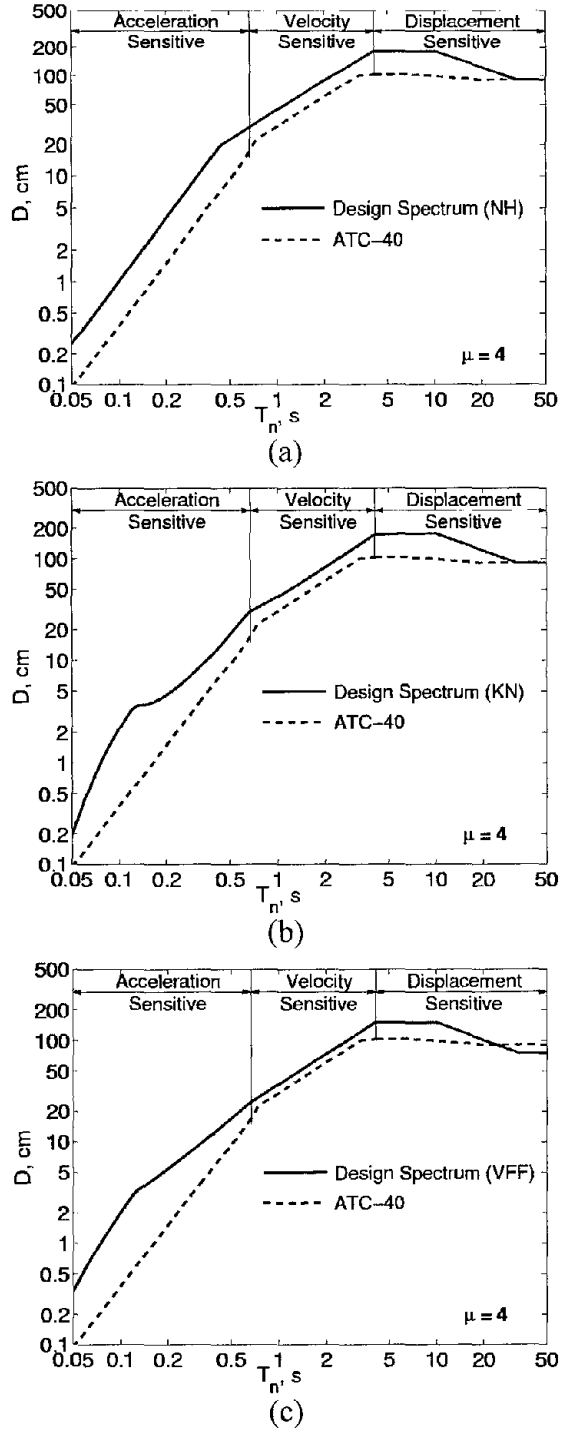

Figure 16. Comparison of deformations computed by ATC-40 procedure with those from three different inelastic design spectra (μ = 4): (a) Newmark and Hall (1982), (b) Krawinkler and Nassar (1992), and (c) Vidic, Fajfar and Fischinger (1994).

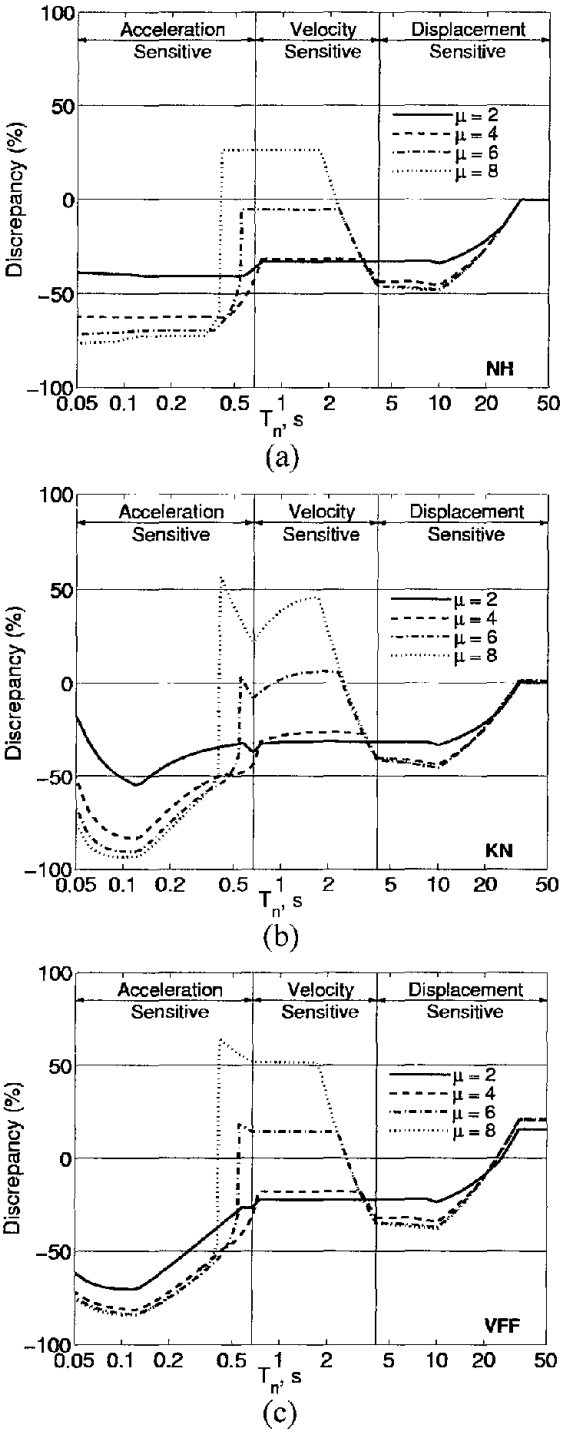

Figure 17. Discrepancy in deformations computed by ATC-40 procedure relative to three different inelastic design spectra: (a) Newmark and Hall (1982), (b) Krawinkler and Nassar (1992), and (c) Vidic, Fajfar and Fischinger (1994).

IMPROVED PROCEDURES

Presented next are two improved procedures that eliminate the errors (or discrepancies) in the ATC-40 procedures, but retain their graphical appeal. Procedures A and B that are presented are akin to ATC-40 Procedures A and B, respectively. The improved procedures use the well-known constant-ductility design spectrum for the demand diagram, instead of the elastic design spectrum for equivalent linear systems in ATC-40 procedures.

INELASTIC DESIGN SPECTRUM

A constant-ductility design spectrum is established by reducing the elastic design spectrum by appropriate ductility-dependent factors that depend on T_n. The earliest recommendation for the reduction factor, R_y (Eq. 12), goes back to the work of Veletsos and Newmark (1960), which is the basis for the inelastic design spectra developed by Newmark and Hall (1982). Starting with the elastic design spectrum of Fig. 7 and these $R_y - \mu$ relations for acceleration-, velocity-, and displacement-sensitive spectral regions, the inelastic design spectrum constructed by the procedure described in Chopra (1995, Section 7.10) is shown in Fig. 18a.

In recent years, several recommendations for the reduction factor have been developed (Krawinkler and Nassar, 1992; Vidic, Fajfar, and Fischinger, 1994; Riddell, Hidalgo, and Cruz, 1989; Tso and Naumoski, 1991; Miranda and Bertero, 1994). Based on two of these recommendations, the inelastic design spectrum is shown in Figs. 18b and 18c. For a fixed $\mu = 2$, the inelastic spectra from Fig. 18 are compared in Fig. 19. The three spectra are very similar in the velocity-sensitive region of the spectrum, but differ in the acceleration-sensitive region. An improved procedure based on such inelastic design spectra is presented in two versions that follow.

INELASTIC DEMAND DIAGRAM

The inelastic design spectra of Fig. 18 will be plotted in the *A-D* format to obtain the corresponding demand diagrams. The peak deformation D of the inelastic system is given by Eq. (11) where A_y is known from Fig. 18 for a given T_n and μ. Determined corresponding to the three inelastic design spectra in Fig. 18, such data pairs (A_y,D) are plotted to obtain the demand diagram for inelastic systems (Fig. 20).

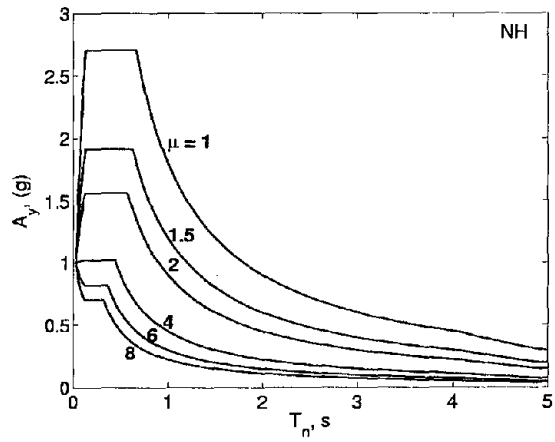

(a)

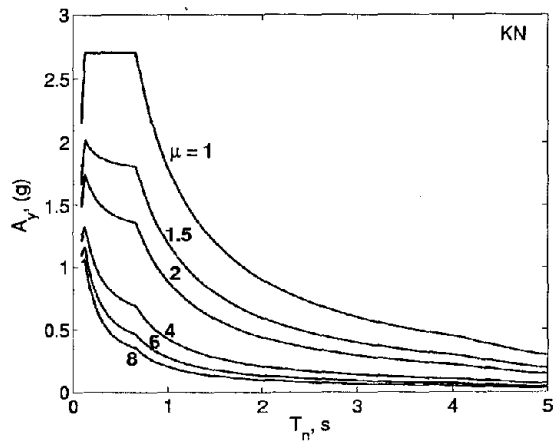

(b)

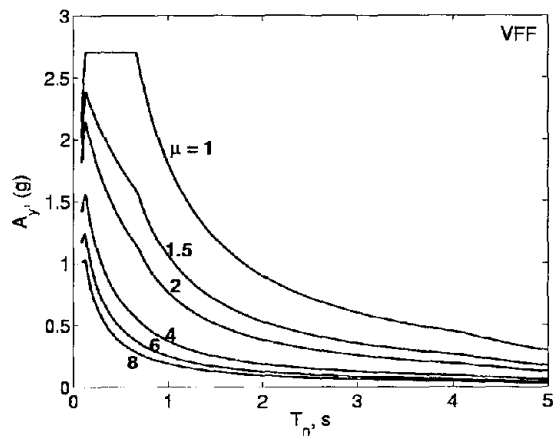

(c)

Figure 18. Inelastic design spectra: (a) Newmark and Hall (1982), (b) Krawinkler and Nassar (1992), and (c) Vidic, Fajfar and Fischinger (1994).

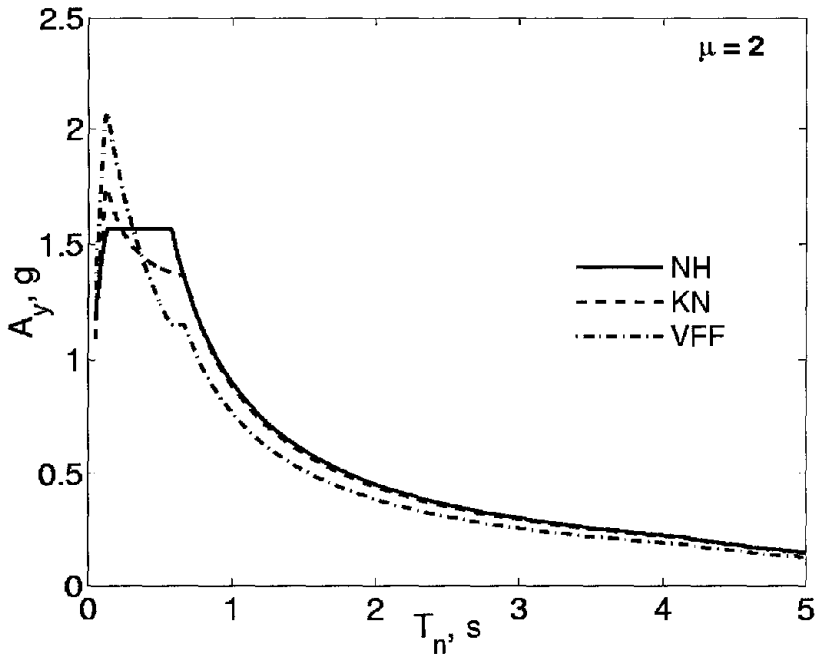

Figure 19. Pseudo-acceleration design spectrum for inelastic systems (μ= 2) using three $R_y - \mu - T_n$ equations: Newmark-Hall (NH), Krawinkler-Nassar (KN), and Vidic-Fajfar-Fischinger (VFF).

PROCEDURE A

This procedure, which uses the demand diagram for inelastic systems (Fig. 20), will be illustrated with reference to six elastoplastic systems defined by two values of T_n = 0.5 and 1.0 sec and three different yield strengths, given by Eq. (8) corresponding to μ = 2, 4, and 6, respectively. Superimposed on the demand diagrams are the capacity diagrams for three inelastic systems with T_n = 0.5 sec (Figs. 21a, 22a, and 23a) and T_n = 1.0 sec (Figs. 21b, 22b, and 23b). The yielding branch of the capacity diagram intersects the demand diagram for several μ values. One of these intersection points, which remains to be determined, will provide the deformation demand. At the one relevant intersection point, the ductility factor calculated from the capacity diagram should match the ductility value associated with the intersecting demand curve. Determined according to this criterion, the deformation for each system is noted in Figs. 21 to 23. Implementation of this procedure is illustrated for two systems.

Examples

The yield deformation of System 1 is u_y = 3.724 cm . The yielding branch of the capacity diagram intersects the demand curves for μ = 1, 2, 4, 6, and 8 at 133.93 cm, 66.96 cm, 33.48 cm, 22.3 cm, and 16.5 cm, respectively (Fig. 21a). Dividing by u_y, the corresponding ductility factors are 133.93÷3.724=35.96 (which exceeds μ = 1 for this demand curve), 66.96÷3.724=17.98 (which exceeds μ = 2 for this demand curve), 33.48÷3.724=8.99 (which exceeds μ = 4 for this demand curve), 22.3÷3.724=6 (which matches μ = 6 for this demand

curve), and 16.5÷3.724=4.43 (which is smaller than $\mu = 8$ for this demand curve). Thus, the ductility demand is 6 and the deformation of System 1 is $D = 22.3$ cm.

For System 3, $u_y = 9.681$cm . The yielding branch of the capacity diagram intersects the demand curve for $\mu = 1$ at 51.34 cm (Fig. 21a). The corresponding ductility factor is 51.34÷9.681=5.3, which is larger than the $\mu = 1$ for this demand curve. The yielding branch of the capacity diagram also intersects the demand curve for $\mu = 2$ continuously from 9.681 cm to 25.2 cm, which correspond to ductility factors of 1 to 2.6. The intersection point at 19.29 cm corresponds to ductility factor = 19.39÷9.681=2 which matches $\mu = 2$ for this demand curve. Thus, the ductility demand is 2 and the deformation of System 3 is $D = 19.39$ cm.

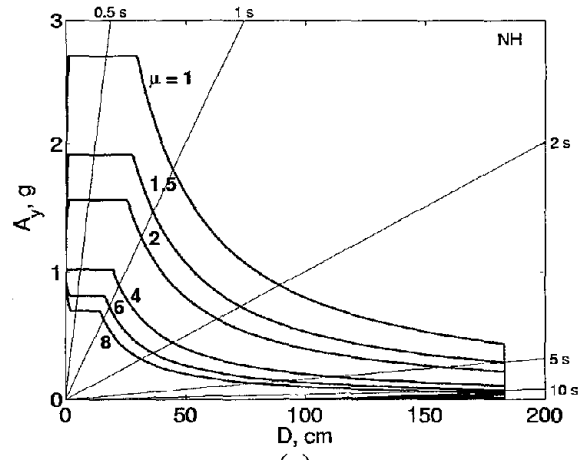

(a)

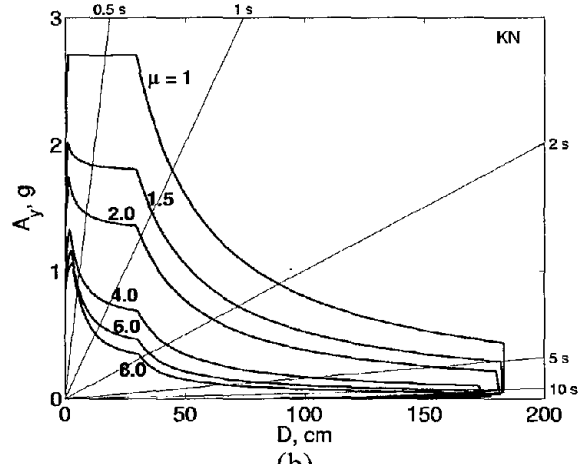

(b)

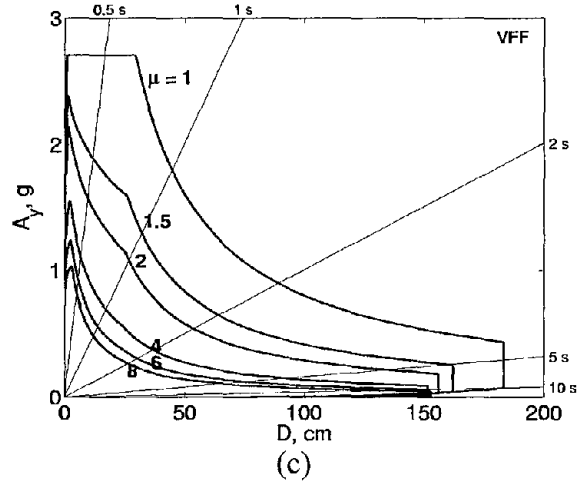

(c)

Figure 20. Inelastic demand diagrams: (a) Newmark and Hall (1982), (b) Krawinkler and Nassar (1992), and (c) Vidic, Fajfar and Fischinger (1994).

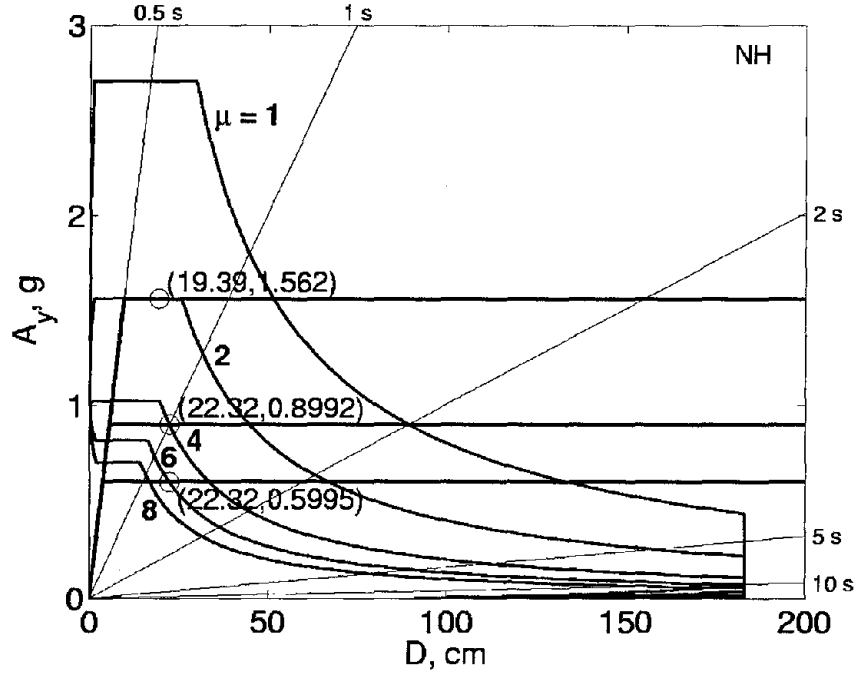

(a)

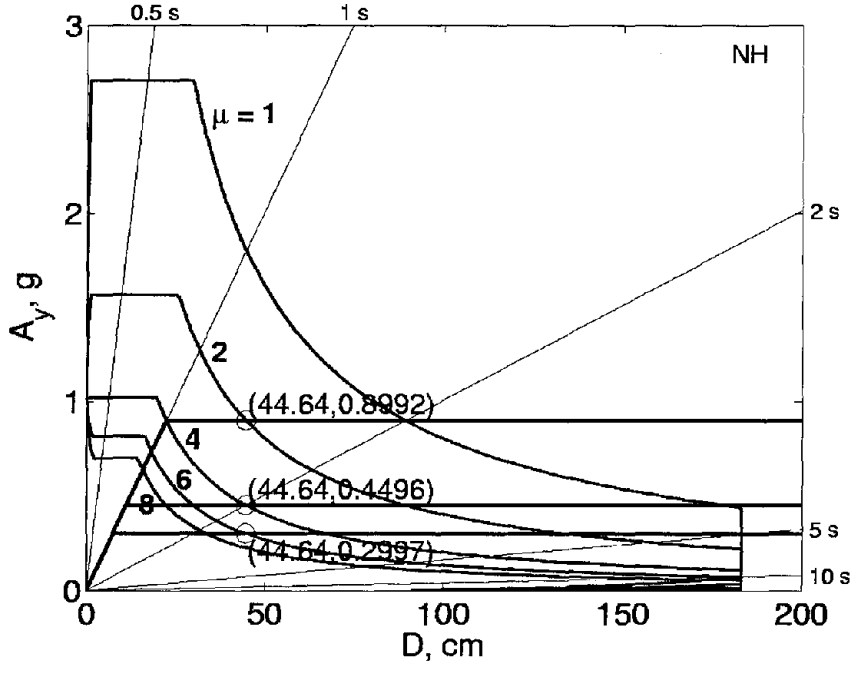

(b)

Figure 21. Application of improved Procedure A using Newmark-Hall (1982) inelastic design spectrum: (a) Systems 1 to 3, and (b) Systems 4 to 6.

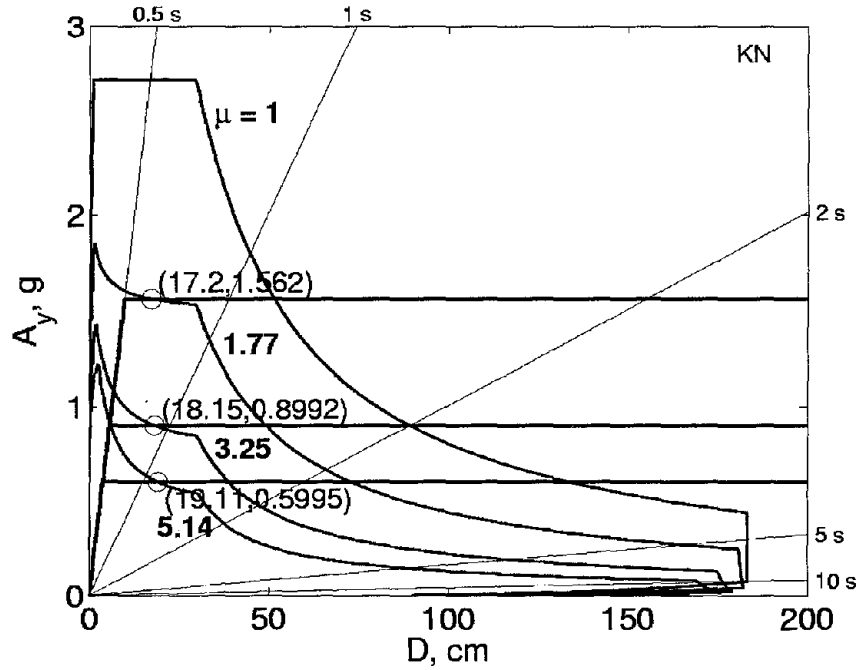

(a)

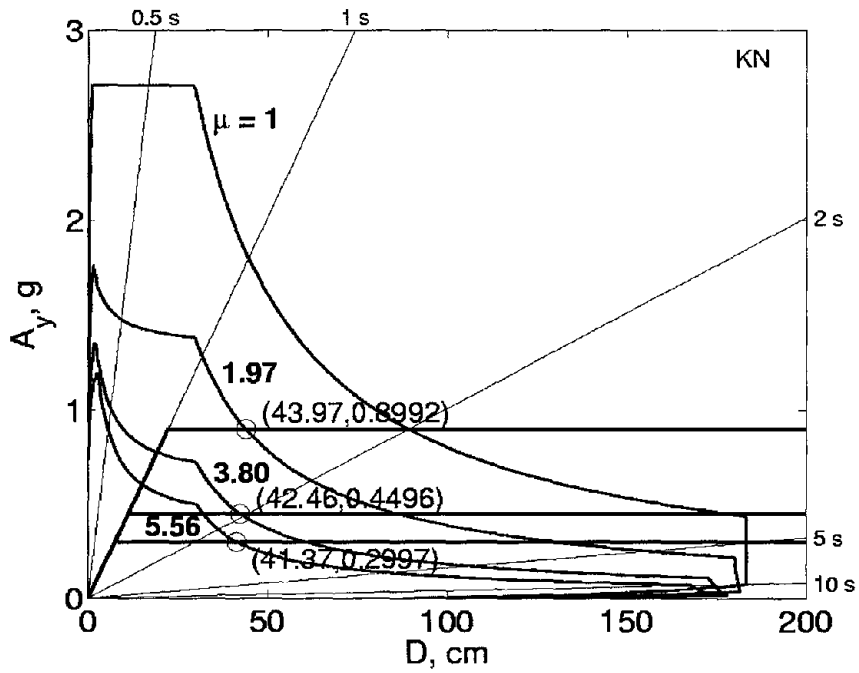

(b)

Figure 22. Application of improved Procedure A using Krawinkler-Nassar (1992) inelastic design spectrum: (a) Systems 1 to 3, and (b) Systems 4 to 6.

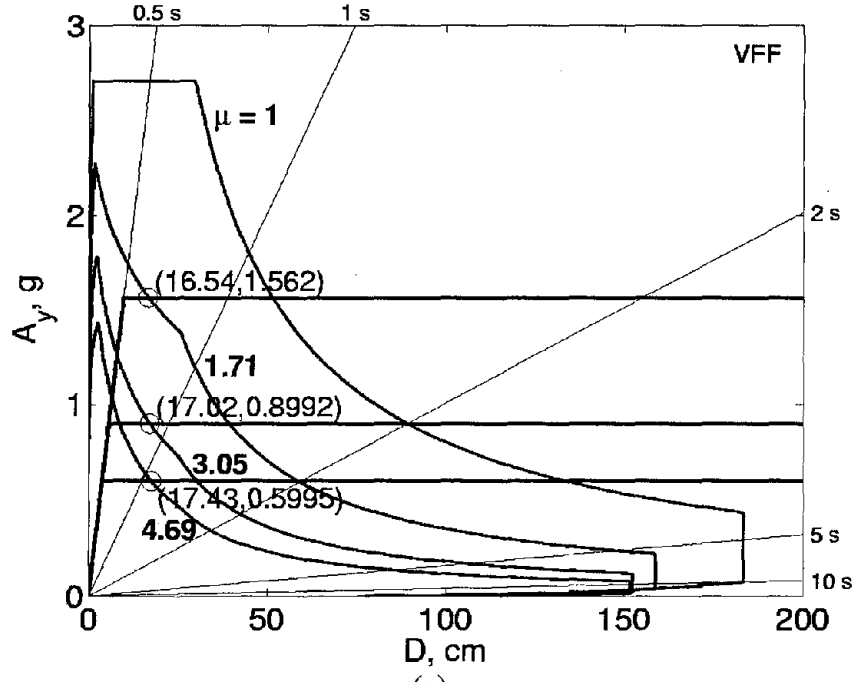

(a)

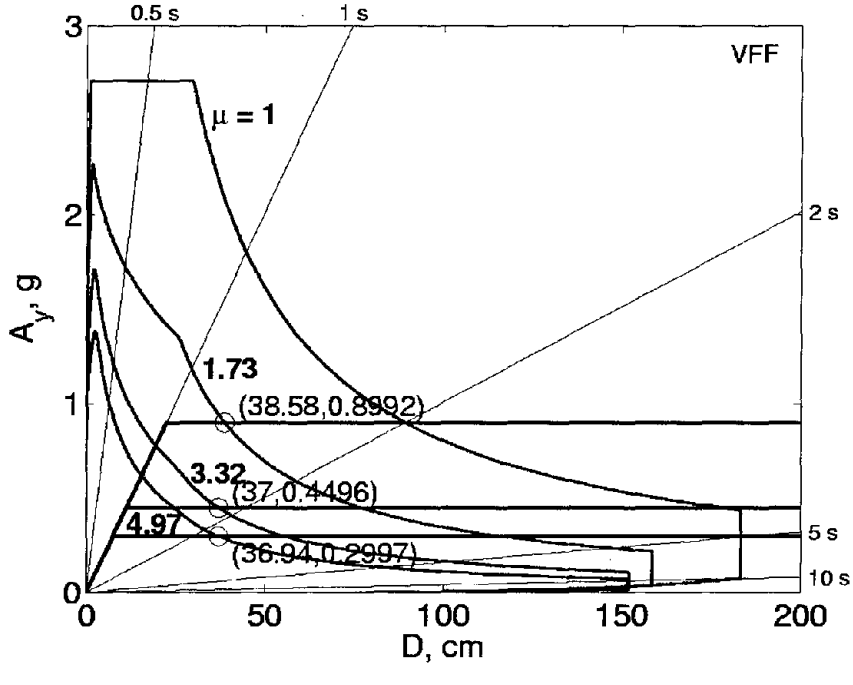

(b)

Figure 23. Application of improved Procedure A using Vidic-Fajfar-Fischinger (1994) inelastic design spectrum: (a) Systems 1 to 3, and (b) Systems 4 to 6.

Observe that for the presented examples, the ductility factor at the intersection point matched exactly the ductility value associated with one of the demand curves because the f_y values were chosen consistent with the same μ values for which the demand curves have been plotted. In general this is not the case and interpolation between demand curves for two μ values would be necessary. Alternatively, the demand curves may be plotted at a finer μ interval avoiding the need for interpolation.

Comparison with ATC-40 Procedure A

The improved procedure just presented gives the deformation value consistent with the selected inelastic design spectrum (Table 15), while retaining the attraction of graphical implementation of the ATC-40 Procedure A. Comparison of Figs. 21 (or 22 or 23) and 5 indicates that the two procedures are similar in the sense that the desired deformation is determined at the intersection of the capacity diagram and the demand diagram. However, the two procedures differ fundamentally in an important sense; the demand diagram used is different: the constant-ductility demand diagram for inelastic systems in the improved procedure (Figs. 21 to 23) versus the elastic demand diagram in ATC-40 Procedure A for equivalent linear systems (Fig. 5).

Observe that equivalent linear systems are analyzed using the elastic design spectrum for a range of damping values, wide enough to cover the large damping expected for equivalent linear systems (Fig. 3). However, most existing rules for constructing elastic design spectra are limited to $\zeta = 0$ to 20% (Chopra, 1995, Section 6.9).

PROCEDURE B

This version of the improved procedure avoids construction of the inelastic design spectrum. The peak deformation D of an inelastic system with properties T_n, ζ, and f_y is determined by the following sequence of steps:

1. Plot the capacity diagram and the 5%-damped elastic demand diagram of Fig. 7 in A-D format.
2. Assume the expected ductility demand μ; start with $\mu = 1$.
3. Determine $A_y(T_n, \zeta, \mu)$ from the inelastic design spectrum for the estimated μ and calculate D from Eq. (14).
4. Plot the point with coordinates D and A_y.
5. Check if the curve generated by connecting similar points intersects the capacity diagram. If not, repeat Steps 3 and 4 with larger values of μ; otherwise go to Step 6.
6. The earthquake-induced deformation demand D is given by the D-value at the intersection point.

Examples

This procedure is implemented for Systems 1 to 6 (Table 5) with the earthquake excitation characterized by the elastic design spectrum of Fig. 7. The results are summarized in Table 15; intermediate results are available in Tables 16 and 17. The inelastic design spectrum of Newmark and Hall (1982) provides the D_y, A_y pairs for $T_n = 0.5$ sec and 1.0 sec in Tables 16 and 17, respectively; and D is determined by Step 3. The (D, A_y) pairs are plotted to obtain the curve *A-B* in Figs. 24a and 24b. The 5%-damped elastic demand diagram and capacity diagrams for the selected systems are also shown; however, a plot of the elastic demand diagram is not essential to the procedure. The intersection point between the curve *A-B* and the capacity diagram gives the system deformation: $D = 22.32$ cm, $D = 22.32$ cm and $D = 19.39$ cm for Systems 1, 2 , and 3, respectively (Fig. 24a) and $D = 44.64$ cm for Systems 4 to 6 (Fig. 24b). In the latter case, the deformation of the inelastic system is independent of the yield strength and equals that of the corresponding linear system because T_n is in the velocity-sensitive spectral region. This is the well-known equal displacement rule.

Comparison with ATC-40 Procedure B

The improved procedure just presented gives the deformation value consistent with the inelastic design spectrum, while retaining the attraction of a graphical implementation of ATC-40-Procedure B. Comparison of Figs. 24 and 11 indicates that the two procedures are graphically similar. However, they differ fundamentally in one important sense. Each point on the curve *A-B* (Fig. 24) in the improved procedure is determined by analyzing an inelastic system. In contrast the ATC-40-Procedure B gives a point on the curve *A-B* (Fig. 11) by analyzing an equivalent linear system.

ALTERNATIVE DEFINITION OF EQUIVALENT DAMPING

We digress briefly to observe that the capacity spectrum method based on the elastic design spectrum has been modified to use an alternative definition of equivalent viscous damping, ζ_{eq} (Freeman, 1998; WJE, 1996). This ζ_{eq} is derived by equating the peak deformation of the equivalent linear system, determined from the elastic design spectrum (Chopra, 1995; Section 6.9), to the peak deformation of the yielding system, determined from the inelastic design spectrum (Chopra, 1995; Section 7.10). The capacity spectrum method, modified in this way, should give essentially the same deformation as the improved procedure. However, we see little benefit in making this detour when the well-known constant-ductility inelastic design spectra can be used directly in the improved procedure.

Table 15. Results from Improved Procedure analysis of six systems for design spectrum.

System	$D_{improved}$ (cm)	$D_{spectrum}$ (cm)	Discrepancy (%)
1	22.32	22.32	0
2	22.32	22.32	0
3	19.39	19.39	0
4	44.64	44.64	0
5	44.64	44.64	0
6	44.64	44.64	0

Table 16. Detailed results from improved Procedure B analysis of Systems 1 to 3 for design spectrum.

μ	D_y (cm)	A_y (g)	D (cm)
1	16.794	2.706	16.794
1.25	13.713	2.21	17.141
1.5	11.875	1.914	17.813
1.75	10.622	1.712	18.588
2	**9.696**	**1.562**	**19.392**
2.25	8.977	1.447	20.198
2.5	8.397	1.353	20.993
2.75	7.917	1.276	21.772
3	7.44	1.199	22.321
3.25	6.868	1.107	22.321
3.5	6.377	1.028	22.321
3.75	5.952	0.959	22.321
4	**5.58**	**0.8992**	**22.321**
4.25	5.252	0.846	22.321
4.5	4.96	0.799	22.321
4.75	4.699	0.757	22.321
5	4.464	0.719	22.321
5.25	4.252	0.685	22.321
5.5	4.058	0.654	22.321
5.75	3.882	0.626	22.321
6	**3.72**	**0.5995**	**22.321**
6.25	3.571	0.575	22.321
6.5	3.434	0.553	22.321
6.75	3.307	0.533	22.321
7	3.189	0.514	22.321

Table 17. Detailed results from improved Procedure B analysis of Systems 4 to 6 for design spectrum.

μ	D_y (cm)	A_y (g)	D (cm)
1	44.642	1.798	44.642
1.25	35.714	1.439	44.642
1.5	29.761	1.199	44.642
1.75	25.51	1.028	44.642
2	**22.321**	**0.8992**	**44.642**
2.25	19.841	0.799	44.642
2.5	17.857	0.719	44.642
2.75	16.233	0.654	44.642
3	14.881	0.599	44.642
3.25	13.736	0.553	44.642
3.5	12.755	0.514	44.642
3.75	11.905	0.48	44.642
4	**11.161**	**0.4496**	**44.642**
4.25	10.504	0.423	44.642
4.5	9.92	0.4	44.642
4.75	9.398	0.379	44.642
5	8.928	0.36	44.642
5.25	8.503	0.343	44.642
5.5	8.117	0.327	44.642
5.75	7.764	0.313	44.642
6	**7.44**	**0.2997**	**44.642**
6.25	7.143	0.288	44.642
6.5	6.868	0.277	44.642
6.75	6.614	0.266	44.642
7	6.377	0.257	44.642

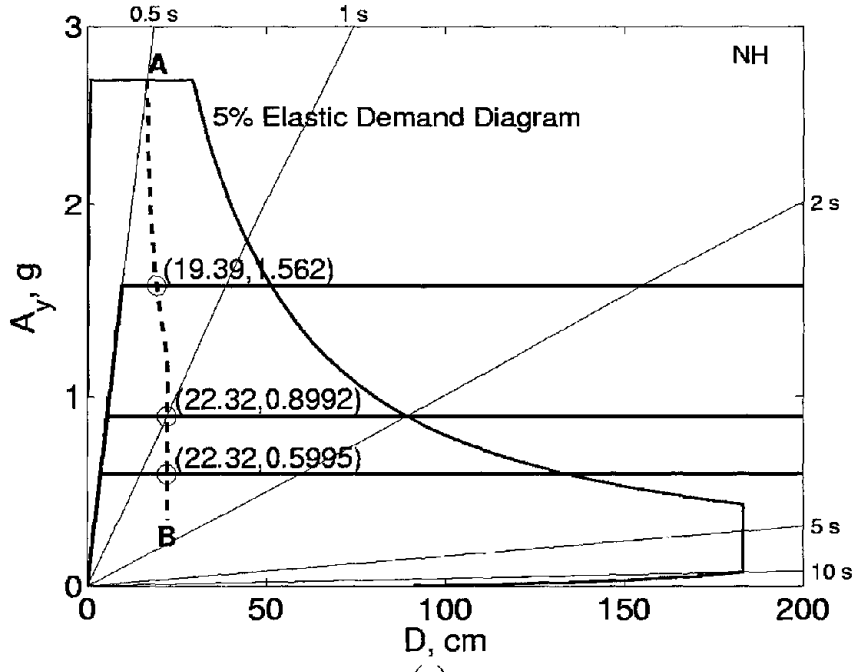

(a)

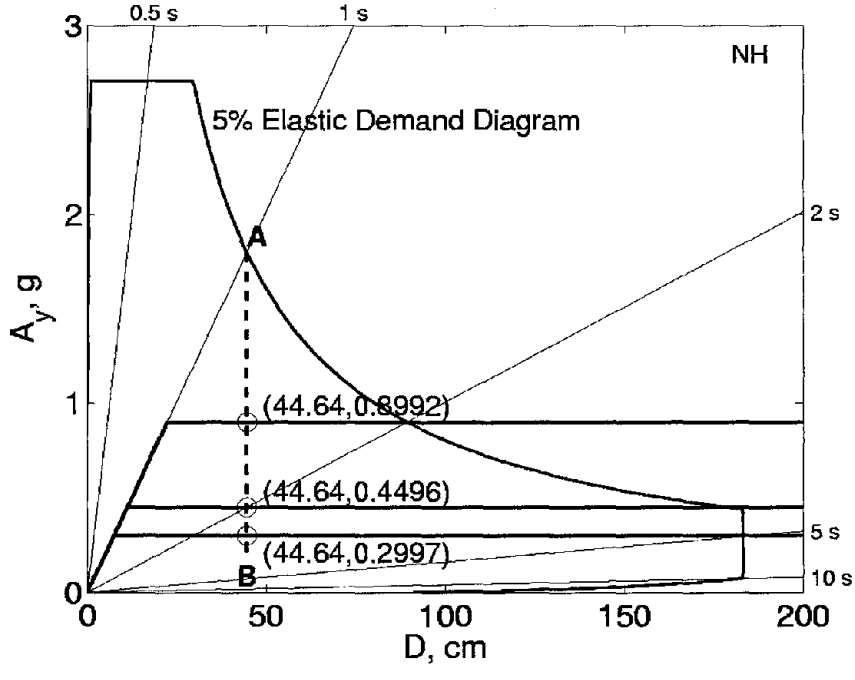

(b)

Figure 24. Application of improved Procedure B using Newmark-Hall (1982) inelastic design spectrum: (a) Systems 1 to 3, and (b) Systems 4 to 6.

IMPROVED PROCEDURE: NUMERICAL VERSION

BASIC CONCEPT

The improved procedures presented in the preceding section were implemented graphically, in part, to highlight the similarities and differences relative to the Nonlinear Static Procedure in the ATC-40 report. The graphical implementation of the first version of the improved procedure is especially attractive as the desired earthquake-induced deformation is determined at the intersection of the capacity and demand diagrams. However, the graphical feature is not essential and the procedure can be implemented numerically. Such a procedure using $R_y - \mu - T_n$ equations is presented in this section.

$R_y - \mu - T_n$ EQUATIONS

The $R_y - \mu - T_n$ equations for elastoplastic systems, consistent with the Newmark-Hall inelastic design spectra are (Chopra, 1995; Section 7.10):

$$R_y = \begin{cases} 1 & T_n < T_a \\ (2\mu - 1)^{\beta/2} & T_a < T_n < T_b \\ \sqrt{2\mu - 1} & T_b < T_n < T_{c'} \\ \dfrac{T_n}{T_c}\mu & T_{c'} < T_n < T_c \\ \mu & T_n > T_c \end{cases} \tag{15a}$$

where

$$\beta = \ln(T_n/T_a)/\ln(T_b/T_a) \tag{15b}$$

and the $T_a, T_b,$ and T_c are defined in Fig. 7 and $T_{c'}$ is the period where the constant-A and constant-V branches of the inelastic design spectrum intersect (Chopra, 1995, Section 7.10). Recasting Eq. (15) gives μ as a function of R_y:

$$\mu = \begin{cases} \text{Undefined} & T_n < T_a \\ \left(1 + R_y^{2/\beta}\right)/2 & T_a < T_n < T_b \\ \left(1 + R_y^2\right)/2 & T_b < T_n < T_{c'} \\ \dfrac{T_c}{T_n} R_y & T_{c'} < T_n < T_c \\ R_y & T_n > T_c \end{cases} \tag{16}$$

For a given R_y, μ can be calculated for all T_n except for $T_b < T_n < T_c$, wherein two possibilities need to be checked since $T_{c'}$ itself depends on μ (see Appendix B).

Based on the earthquake response of bilinear systems, Krawinkler and Nassar (1992) have developed the following $R_y - \mu - T_n$ equations:

$$R_y = [c(\mu-1)+1]^{1/c} \tag{17}$$

where

$$c(T_n,\alpha) = \frac{T_n^a}{1+T_n^a} + \frac{b}{T_n} \tag{18}$$

and the numerical coefficients depend on the slope αk of the yielding branch (Fig. 2a): $a = 1$ and $b = 0.42$ for $\alpha = 0\%$; $a = 1$ and $b = 0.37$ for $\alpha = 2\%$; $a = 0.8$ and $b = 0.29$ for $\alpha = 10\%$. Recasting Eq. (18) provides μ as a function of R_y:

$$\mu = 1 + \frac{1}{c}(R_y^c - 1) \tag{19}$$

For given values of R_y and α, μ can be calculated from Eq. (19).

Based on the earthquake response of bilinear systems, Vidic, Fajfar and Fischinger (1994) have developed the following $R_y - \mu - T_n$ equations:

$$R_y = \begin{cases} 1.35(\mu-1)^{0.95}\dfrac{T_n}{T_o} + 1 & T_n \le T_o \\ 1.35(\mu-1)^{0.95} + 1 & T_n > T_o \end{cases} \tag{20}$$

where

$$T_o = 0.75\mu^{0.2} T_c \le T_c \tag{21}$$

Recasting Eq. (20) gives μ as a function of R_y:

$$\mu = \begin{cases} 1 + \left[0.74(R_y-1)\dfrac{T_o}{T_n}\right]^{1.053} & T_n \le T_o \\ 1 + [0.74(R_y-1)]^{1.053} & T_n > T_o \end{cases} \tag{22}$$

Since T_o in Eq. (22) depends on μ (Eq. 21), the value of μ corresponding to a given R_y is determined by solving a nonlinear equation iteratively unless the simpler relation, $T_o = T_c$, is assumed.

Figure 25 shows plots of R_y v's T_n for selected values of μ based on Eqs. (15), (17) for $\alpha = 0$, and (20). In Fig. 26, μ is plotted against T_n from Eqs. (16), (19) for $\alpha = 0$, and (22). Observe the similarity among the three sets of results, indicating consensus among different researchers.

The peak deformation of systems 1 to 6 (Table 5) are determined from Eq. (14) using $R_y - \mu - T_n$ relations of Eq. (16), (19), and (22). Detailed calculations are presented in Appendix B and the results are summarized in Table 18. Observe that the deformation values computed using $R_y - \mu - T_n$ equations are identical to those determined by the graphical procedure (Figs. 21 to 23) except for round-off differences.

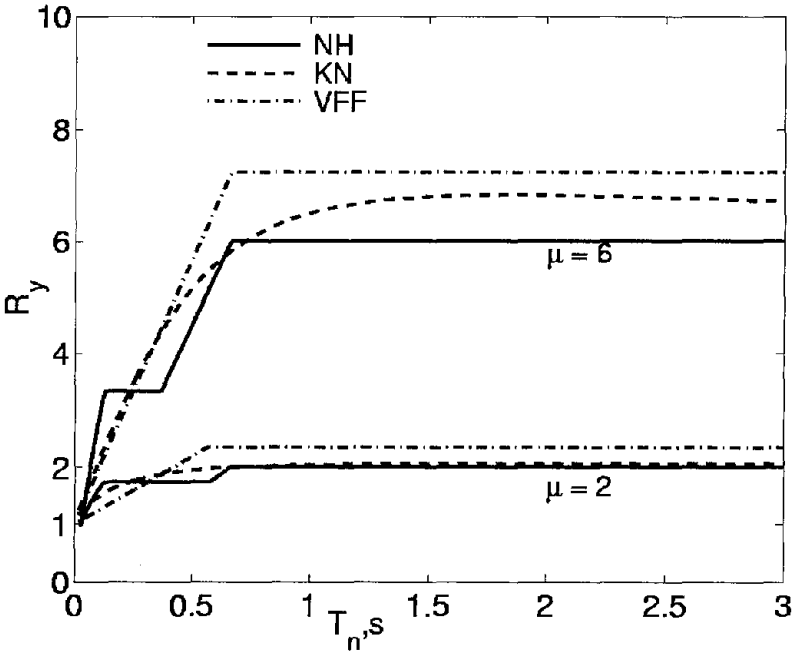

Figure 25. Variation of R_y with T_n for selected ductility values based on three different sources: Newmark and Hall (1982), Krawinkler and Nassar (1992), and Vidic, Fajfar, and Fischinger (1994).

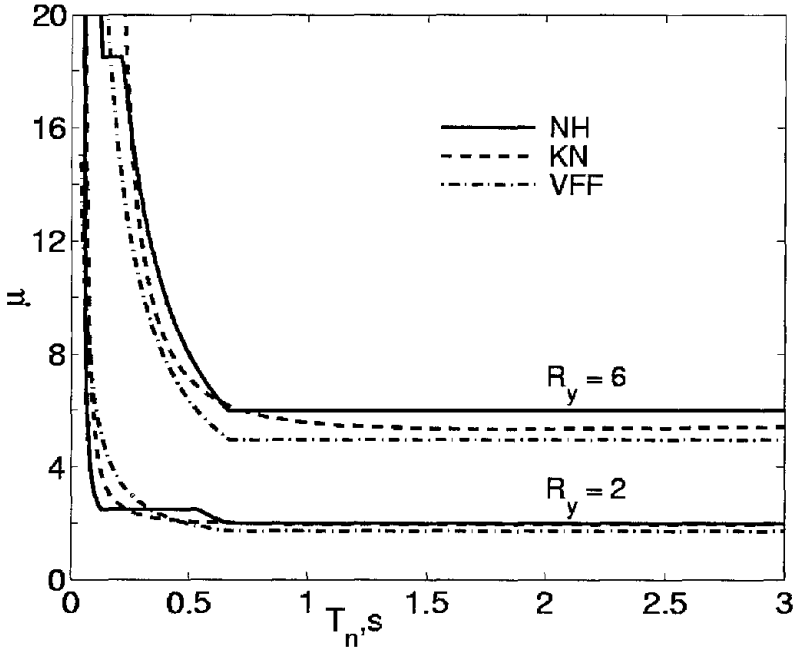

Figure 26. Variation of μ with T_n for selected R_y values based on three different sources: Newmark and Hall (1982), Krawinkler and Nassar (1992), and Vidic, Fajfar, and Fischinger (1994).

Table 18. Results from numerical implementation of improved procedure using three $R_y - \mu - T_n$ equations.

System Properties						Newmark-Hall		Krawinkler-Nassar		Vidic et al.	
System	T_n (s)	A (g)	A_y ($f_y \div w$) (g)	$D_y = u_y$ (cm)	R_y ($A \div A_y$)	μ (Eq. 16)	D ($\mu \times D_y$) (cm)	μ (Eq. 19)	D ($\mu \times D_y$) (cm)	μ (Eq. 22)	D ($\mu \times D_y$) (cm)
1	0.5	2.7062	0.5995	3.7202	4.51	5.99	22.29	5.14	19.11	4.69	17.43
2			0.8992	5.5803	3.01	3.99	22.29	3.25	18.15	3.05	17.02
3			1.5624	9.6962	1.73	2.00	19.39	1.77	17.20	1.71	16.54
4	1	1.7984	0.2997	7.4403	6.00	6.00	44.64	5.56	41.37	4.97	36.94
5			0.4496	11.160	4.00	4.00	44.64	3.80	42.46	3.32	37.00
6			0.8992	22.321	2.00	2.00	44.64	1.97	43.97	1.73	38.58

CONSISTENT TERMINOLOGY

Many new terms that have been introduced in connection with simplified analysis of inelastic systems are examined in this section and, where necessary, better terminology is recommended:

1. *Demand Spectrum.* The term "spectrum" has traditionally implied a function of frequency or period. For example, *response spectrum* is a plot of the peak value of a response quantity as a function of the natural vibration period (or frequency) of the SDF system. Another example: *Fourier Spectrum* of ground acceleration is a plot of the amplitude of the Fourier transform of the excitation against exciting frequency. The "Response Spectrum" terminology was introduced in the 1930s within the context of earthquake engineering, whereas the "Fourier Spectrum" terminology has existed for much longer. Given this background, "spectrum" is inappropriate to describe a plot of pseudo-acceleration v's deformation. The terminology *Demand Diagram* has therefore been used in this investigation.

2. *Capacity Spectrum.* For the same reasons, the recommended terminology is *Capacity Diagram.*

3. *Acceleration-Displacement Response Spectrum (ADRS) Format.* For the same reasons, the recommended terminology is *A-D format.*

4. *Nonlinear Static Procedure (NSP).* The capacity diagram is determined by nonlinear static analysis of the structure, but the demand diagram is determined by dynamic analysis. Because the NSP involves use of both diagrams, the NSP terminology is inappropriate and the suggested alternative is *Simplified Dynamic Analysis.*

5. *Modal Participation Factor.* This traditional terminology for Γ_n (Eq. 1) implies that it is a measure of the degree to which the n^{th} mode participates in the response. However, this is misleading because Γ_n is not independent of how the mode is normalized, nor a measure of the modal contribution to a response quantity (Chopra, 1995; section 13.1).

CONCLUSIONS

This investigation of capacity-demand-diagram methods to estimate the earthquake-induced deformation of inelastic SDF systems has led to the following conclusions:

1. Based on the belief that the deformation of an inelastic system can be estimated by an iterative method requiring analysis of a sequence of equivalent linear systems, the ATC-40 Procedure A did not converge for some of the systems analyzed. It converged in many cases but not to the exact deformation determined by nonlinear response history analysis of the inelastic system, nor to the value determined from the inelastic design spectrum. Thus, convergence of this iterative procedure is deceptive because it can leave the erroneous impression that the calculated deformation is accurate. This approximate procedure therefore does not meet the basic requirement of a rational iterative procedure: it should always converge to the "exact" result after a sufficient number of iterations.

2. The ATC-40 Procedure B always gives a unique value of deformation, the same as determined by Procedure A if it converged.

3. The peak deformation of inelastic systems, determined by ATC-40 procedures, when compared against results of nonlinear response history analysis for several ground motions were shown to be inaccurate. The approximate procedure underestimates significantly the deformation for a wide range of T_n values with errors approaching 50%, implying that the estimated deformation is only about half of the "exact" value.

4. The damping modification factor, κ, in ATC-40 procedures improves the deformation estimate only marginally. Therefore the κ factor is not attractive, especially because it is based primarily on judgement.

5. The ATC-40 procedures were implemented for a wide range of T_n and μ values with the excitation characterized by an elastic design spectrum. The resulting estimate of deformation for the inelastic system was compared with the deformation determined from the inelastic design spectrum using three different $R_y - \mu - T_n$ equations (Newmark and Hall, 1982; Krawinkler and Nassar, 1992; Vidic, Fajfar, and Fischinger, 1994), all of which provided similar results. Relative to these "reference" values, the approximate procedure significantly underestimates the deformation for a wide range of T_n and μ values.

6. The ATC-40 procedures are deficient relative to even the *elastic* design spectrum in the velocity-sensitive and displacement-sensitive regions of the spectrum. For T_n in these regions, the peak deformation of an inelastic system can be estimated from the elastic design spectrum using the well-known equal displacement rule. However, the approximate procedure requires analyses of several equivalent linear systems and still produces worse results.

7. An improved capacity-demand-diagram method that uses the well-known constant-ductility design spectrum for the demand diagram has been developed and illustrated by examples. When both capacity and demand diagrams are plotted in the *A-D* format, the yielding branch of the capacity diagram intersects the demand curves for several μ values. The deformation is given by the one intersection point where the ductility factor calculated from the capacity diagram matches the value associated with the intersecting demand curve. This method gives the deformation value consistent with the selected inelastic design spectrum, while retaining the attraction of graphical implementation of the ATC-40 methods.

8. One version of the improved method is graphically similar to ATC-40 Procedure A. However, the two differ fundamentally in an important sense; the demand diagram used is different: the constant-ductility demand diagram for inelastic systems in the improved procedure versus the elastic demand diagram in Procedure A for equivalent linear systems.

9. A second version of the improved method is graphically similar to ATC-40 Procedure B. However the two differ fundamentally in one important sense. Each point on curve A-B is determined by analyzing an inelastic system in the improved procedure (Fig. 24) but an equivalent linear system in Procedure B (Fig. 12).

10. The improved method can be conveniently implemented numerically if its graphical features are not important to the user. Such a procedure, based on equations relating R_y and μ for

different T_n ranges, has been presented. It has been illustrated by examples using three different $R_y - \mu - T_n$ relations (Newmark and Hall, 1982; Krawinkler and Nassar, 1992; Vidic, Fajfar, and Fischinger, 1994). The graphical and numerical implementations of the improved method are shown to give essentially identical values for deformation.

11. The new terminology that has been introduced in recent years in connection with simplified analysis of inelastic systems has been examined and, where necessary, better terminology recommended:

    (a) The term "spectrum" implies a function of frequency or period (e.g., response spectrum or Fourier spectrum) and is therefore inappropriate to describe a plot of pseudo-acceleration versus deformation. The recommended terminology is *Demand Diagram* and *Capacity Diagram* instead of *Demand Spectrum* and *Capacity Spectrum.*

    (b) *Acceleration-Displacement Response Spectrum (ADRS) Format* is inappropriate for the same reason and *A-D Format* is preferable.

    (c) *Nonlinear Static Procedure* (NSP) is a misleading term because the NSP uses a demand diagram determined by dynamic analysis. The suggested alternative is *Simplified Dynamic Analysis*.

NOTATION

α	strain hardening ratio
a	constant used in Krawinkler and Nassar $R_y - \mu - T_n$ equations
β	constant used in Newmark and Hall $R_y - \mu - T_n$ equations
A	pseudo-acceleration spectrum ordinate
A_i	$(2\pi/T_n)^2 D_i$, pseudo-acceleration corresponding to D_i
A_j	$(2\pi/T_n)^2 D_j$, pseudo-acceleration corresponding to D_j
A_y	$(2\pi/T_n)^2 D_y$, pseudo-acceleration corresponding to yield deformation D_y
b	constant used in Krawinkler and Nassar $R_y - \mu - T_n$ equations
c	variable used in Krawinkler and Nassar $R_y - \mu - T_n$ equations
D	deformation spectrum ordinate
D_{approx}	peak deformation computed from approximate procedure
D_{exact}	exact peak deformation determined by nonlinear response history analysis
$D_{spectrum}$	exact peak deformation determined by inelastic design spectrum
D_i	deformation estimate at the beginning of an iteration
D_j	deformation estimate at the end of an iteration
D_y	yield deformation = u_y
E_D	energy dissipated in inelastic system (= area of hysteresis loop)
E_S	strain energy of the equivalent linear system
ϕ_1	fundamental mode
ϕ_{j1}	j^{th} floor element of the fundamental mode ϕ_1
f_o	minimum strength required for a system to remain elastic
f_y	yield strength
g	acceleration due to gravity
Γ_1	fundamental mode factor defined by Eq. (1)
k	initial elastic stiffness of the inelastic system
k_{sec}	secant stiffness of the equivalent linear system

κ	damping modification factor specified in ATC-40
m	mass of the system
m_j	lumped mass at the jth floor level
M_1^*	effective modal mass for the fundamental vibration mode
N	number of floors
μ	ductility factor
R_y	yield reduction factor
$T_a, T_b, T_c, T_{c'}, T_d, T_e, T_f$	periods that define spectral regions
T_o	transition period used in Vidic, Fajfar, and Fischinger $R_y - \mu - T_n$ equations
T_{eq}	equivalent vibration period
T_n	natural vibration period
u	deformation
$u_{go}, \dot{u}_{go}, \ddot{u}_{go}$	peak ground displacement, velocity, and acceleration
u_m	peak deformation of inelastic system
u_y	yield displacement
V_y	pseudo-velocity corresponding to yield deformation D_y
w	weight of the system
ζ	viscous damping ratio of linearly elastic system
ζ_{eq}	equivalent viscous damping ratio
$\hat{\zeta}_{eq}$	viscous damping used in equivalent linear procedures

REFERENCES

Applied Technology Council (1996). *Seismic evaluation and retrofit of concrete buildings*. Report ATC 40. November.

Bertero, V. V. (1995). Tri-service manual methods. In *Vision 2000*, Part 2, App. J. Sacramento, Calif.: Structural Engineers Assn. of California.

Chopra, A. K. (1995). *Dynamics of structures: theory and applications to earthquake engineering*, Chaps. 3, 6, 7, and 19. Englewood Cliffs, N.J.: Prentice Hall.

Deierlein, G. G., and Hsieh, S-H. (1990). Seismic response of steel frames with semi-rigid connections using the capacity spectrum method. *Proceedings of 4th U.S. National Conference on Earthquake Engineering* 2:863-72.

Fajfar, P. (1998). *Capacity spectrum method based on inelastic demand spectra*. IKIPR Report EE 3/98. September. Ljubljana, Slovenia: Univ. of Ljubljana.

Fajfar, P. (1999). Capacity spectrum method based on inelastic spectra. *Earthquake Engineering and Structural Dynamics* (forthcoming).

FEMA (1997). *NEHRP guidelines for the seismic rehabilitation of buildings,* FEMA 273; and *NEHRP commentary on the guidelines for the seismic rehabilitation of buildings*, FEMA 274. October. Washington, D.C.: Federal Emergency Management Agency.

Freeman, S. A., Nicoletti, J. P., and Tyrell, J. V. (1975). Evaluations of existing buildings for seismic risk — A case study of Puget Sound Naval Shipyard, Bremerton, Washington. *Proceedings of 1st U.S. National Conference on Earthquake Engineering*, 113-22. Berkeley, Calif.: EERI

Freeman, S. A. (1978). Prediction of response of concrete buildings to severe earthquake motion. *Publication SP-55,* 589-605. Detroit, Mich.: American Concrete Inst.

Freeman, S. A. (1998). Development and use of capacity spectrum method. *Proceedings of 6th U.S. National Conference on Earthquake Engineering*, Seattle. CD-ROM. Oakland, Calif.: EERI.

Gulkan, P., and Sozen, M. A. (1974). Inelastic responses of reinforced concrete structures to earthquake motions. *Journal of the American Concrete Inst.* 71(12):604-10.

Hudson, D. E. (1965). Equivalent viscous friction for hysteretic systems with earthquake-like excitations. P*roceedings of Third World Conference on Earthquake Engineering* II:185-202.

Iwan, W. D., and Gates, N. C. (1979a). Estimating earthquake response of simple hysteretic structures. *Journal of the Engineering Mechanics Div.*. 105 (EM3):391-405. ASCE

Iwan, W. D., and Gates, N. C. (1979b). The effective period and damping of a class of hysteretic structures. *Earthquake Engineering and Structural Dynamics* 7(3):199-212.

Jennings, P. C. (1968). Equivalent viscous damping for yielding structures. *Journal of the Engineering Mechanics Div.* 94 (EM1):103-116. ASCE.

Kowalsky, M. J., Priestley, M. J. N., and Macrae, G. A. (1995). Displacement-based design of RC bridge columns in seismic regions. *Earthquake Engineering and Structural Dynamics* 24(12): 1623-43.

Krawinkler, H., and Nassar, A. A. (1992). Seismic design based on ductility and cumulative damage demands and capacities. *Nonlinear Seismic Analysis and Design of Reinforced Concrete Buildings*, eds P. Fajfar and H. Krawinkler. New York: Elsevier Applied Science.

Miranda, E., and Bertero, V. V. (1994). Evaluation of strength reduction factors for earthquake-resistant design. *Earthquake Spectra* 10(2): 357-79.

Moehle, J. P. (1992). Displacement-based design of R/C structures subjected to earthquakes. *Earthquake Spectra* 8(3): 403-427.

Newmark, N. M., and Hall, W. J. (1982). *Earthquake Spectra and Design.* Berkeley, Calif. Earthquake Engineering Research Inst.

Paret, T. F., Sasaki, K. K., Eilbekc, D. H., and Freeman, S. A. (1996). Approximate inelastic procedures to identify failure mechanisms from higher mode effects. Paper No. 966, *11th World Conference on Earthquake Engineering.* Acapulco, Mexico.

Reinhorn, A. M., Li, C., and Constantinou, M. C. (1995). *Experimental and analytical investigations of seismic retrofit of structures with supplemental damping.* Report No. NCEER-95-0001. State Univ. of New York at Buffalo.

Reinhorn, A. M. (1997). Inelastic analysis techniques in seismic evaluations. *Seismic design methodologies for the next generation of codes*, eds. P. Fajfar and H. Krawinkler, 277-87. Rotterdam: Balkema.

Riddell, R., Hidalgo, P., Cruz, E. (1989). Response modification factors for earthquake resistant design of short period buildings. *Earthquake Spectra* 5(3):571-90.

Shibata, A., and Sozen, M. A. (1976). Substitute structure method for seismic design in R/C. *Journal of the Structural Division* 102(ST1):1-18. ASCE.

Tso, W. K., Naumoski, N. (1991). Period-dependent seismic force reduction factors for short-period structures. *Canadian Journal of Civil Engineering* 18(4):568-74.

Tsopelas, P., Constantinou, M. C., Kircher, C. A., and Whittaker, A. S. (1997). *Evaluation of simplified methods of analysis for yielding structures.* Report No. NCEER-97-0012, State Univ. of New York at Buffalo.

Veletsos, A. S., and Newmark, N. M. (1960). Effects of inelastic behavior on the response of simple system to earthquake motions. *Proceedings of the 2nd World Conference on Earthquake Engineering*, Japan 2:895-912.

Vidic, T., Fajfar, P., and Fischinger, M. (1994). Consistent inelastic design spectra: strength and displacement. *Earthquake Engineering and Structural Dynamics* 23(5) 507-521.

Wallace, J. W. (1995). Displacement-based design of R/C structural walls. *Proceedings of 10th European Conference on Earthquake Engineering* 3:1539-144.

WJE. (1996). *Seismic Dynamic Analysis for Buildings*. Final Manuscript prepared for the U.S. Army Engineering Division by Wiss, Janey, Elstner Assocs. Inc. Emeryville, Calif. (Unpublished).

APPENDIX A. DEFORMATION OF VERY-SHORT PERIOD SYSTEMS BY ATC-40 PROCEDURE B

Consider an elastoplastic system with the following properties: $T_n = 0.1s$, ζ = 5%, $f_y = 0.2659w$, $u_y = 0.066\text{cm}$. The deformation demand of this system computed from ATC-40 Procedure B is $D = 2.267\text{cm}$ (Fig. A.1a) and the values of $T_{eq} = 0.5861s$ and $\hat{\xi}_{eq} = 0.397$. The "exact" deformation of this system computed from nonlinear RHA is 0.3944 cm and the error is $100 \times (2.267 - 0.3944) \div 0.3944 = 475\%$. Clearly ATC-40 Procedure B leads to unreasonably large error for such a system.

Figure A.1b shows the close-up view of the intersection between curve *A-B* and the capacity diagram wherein the demand diagrams for 5% and 39.7% damping are also included. Observe that the demand diagram for 39.7% damping also passes through the intersection point between curve *A-B* and the capacity diagram. This figure leads to the following observations.

The curve *A-B* can be divided into three distinct segments. Initially the curve is very steep, it then becomes essentially flat, and finally it begins to move downward slowly. Since the capacity of the selected system is lower than the flat portion of the curve *A-B*, the intersection between the capacity diagram and the curve *A-B* does not occur till the third segment. On the 39.7% demand curve, the intersection occurs past the constant pseudo-acceleration region of the spectrum. This implies that even though the initial elastic period of the system is in the very-short period region, the intersection would occur in the constant-*V* region if the capacity of the system is smaller than the pseudo-acceleration value in the constant-*A* region of the response spectrum corresponding to $\hat{\xi}_{eq} = 0.397$. As a result, the equivalent period at this intersection point would have to be significantly larger than the initial elastic period (for the selected system $T_n = 0.1s$ and $T_{eq} = 0.5861s$) which in turn would lead to large deformation demand.

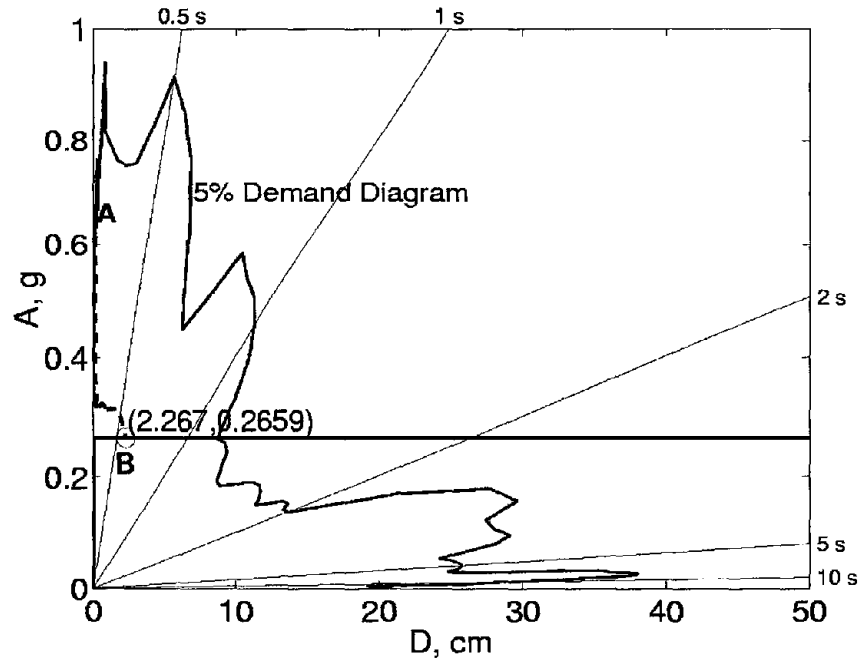

(a)

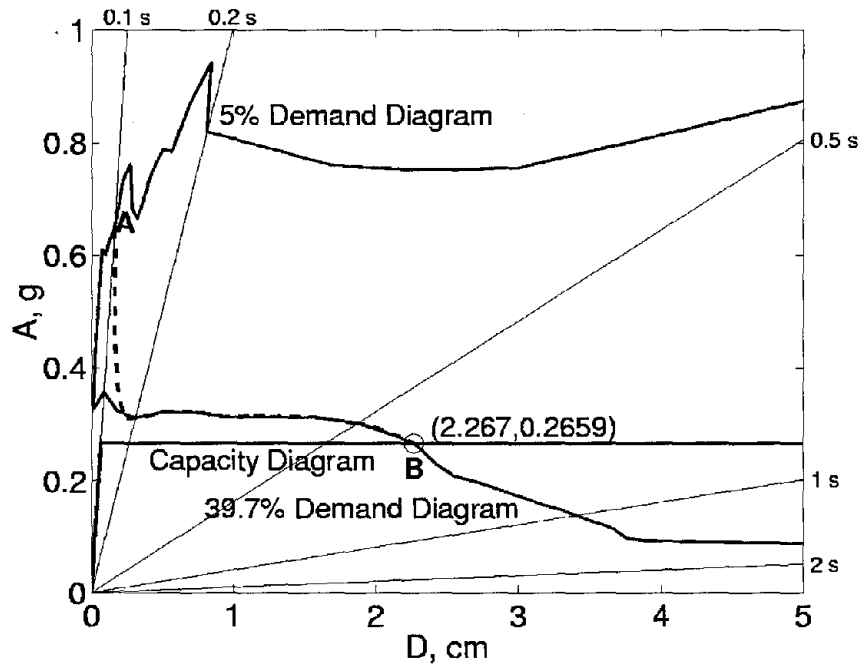

(b)

Figure A.1. ATC-40 Procedure B applied to a system with T_n = 0.1s and A_y = 0.2659 g: (a) deformation demand; and (b) close-up view near the intersection between the demand and capacity diagrams.

APPENDIX B: EXAMPLES USING $R_y-\mu-T_n$ EQUATIONS

SYSTEM 1

Consider an elastoplastic system with the following properties: $T_n=0.5s$, ζ = 5%, $A_y=f_y\div w=0.5995g$. The pseudo-acceleration for linear-elastic system with $T_n=0.5s$, $\zeta=5\%$ is $A=2.7062g$. For this system, $D_y=u_y=(2\pi/T_n)^2\times A_y\times g=(2\pi/0.5)^2\times 0.5995\times 980$ = 3.7202 cm and $R_y=2.7062\div 0.5995=4.51$.

Newmark-Hall Equation (Eq. 16)

The periods corresponding to various regions of the Newmark-Hall design spectrum are $T_a=1/33s$, $T_b=0.125s$, and $T_c=0.6634s$; $T_{c'}$ is unknown at this time because it depends on μ that is yet to be determined. Since $T_{c'}$ is unknown, it is not clear which equation — the third or the fourth in Eq. (16) — should be used to determine μ. Assuming that $T_b<T_n<T_{c'}$, gives $\mu=(1+R_y^2)\div 2=(1+4.51^2)\div 2=10.67$. For this value of μ, $T_{c'}=T_c\sqrt{2\mu-1}/\mu$ $=0.6634\sqrt{2\times 10.67-1}/10.67=0.2804$ s. Clearly the assumption that $T_b<T_n<T_{c'}$ is not correct. Therefore, we must use the available equation for $T_{c'}<T_n<T_c$, which gives $\mu=R_y\times T_c\div T_n$ $=4.51\times 0.6634\div 0.5=5.99$. For this value of μ, $T_{c'}=0.6634\sqrt{2\times 5.99-1}/5.99$ = 0.3674 s and the assumption that $T_b<T_n<T_{c'}$ is valid. The deformation demand $D=5.99\times 3.7202=$ 22.29 cm.

Krawinkler-Nassar Equation (Eq. 19)

For elastoplastic force-deformation behavior, a=1 and b=0.42. Then $c=0.5\div(1+0.5)+0.42\div 0.5=1.1733$ (Eq. 18) and $\mu=1+(1\div 1.1733)\times(4.51^{1.1733}-1)$ = 5.14. The deformation demand $D=5.14\times 3.7202=$ 19.11 cm.

Vidic-Fajfar-Fischinger Equation (Eq. 22)

Since μ is unknown at this time, T_o (Eq. 21) can not be determined at this time. Assume that $T_o=T_c=0.6634s$ (Fajfar 1998), $T_n=0.5s<T_o$. The first of the two equations in Eq. (22) then gives $\mu=1+[0.74\times(0.6634/0.5)(4.51-1)]^{1.053}=4.69$. The deformation demand $D=$ $4.69\times 3.7202=$ 17.43 cm.

SYSTEM 2

Consider an elastoplastic system with the following properties: $T_n=0.5s$, ζ = 5%, $A_y=f_y\div w=0.8992g$. The pseudo-acceleration for linear-elastic system with $T_n=0.5s$, $\zeta=5\%$

is $A = 2.7062g$. For this system, $D_y = u_y = (2\pi/T_n)^2 \times A_y \times g = (2\pi/0.5)^2 \times 0.8992 \times 980 = 5.5803$ cm and $R_y = 2.7062 \div 0.8992 = 3.01$.

Newmark-Hall Equation (Eq. 16)

Assuming that $T_b < T_n < T_{c'}$, gives $\mu = (1 + 3.01^2) \div 2 = 5.03$. For this value of μ, $T_{c'} = 0.6634 \times \sqrt{2 \times 5.03 - 1} / 5.03 = 0.3970$ s. Clearly the assumption that $T_b < T_n < T_{c'}$ is not correct. Therefore, we must use the available equation for $T_{c'} < T_n < T_c$, which gives $\mu = 3.01 \times 0.6634 \div 0.5 = 3.99$. For this value of μ, $T_{c'} = 0.6634\sqrt{2 \times 3.99 - 1}/3.99 = 0.4393$ s and the assumption that $T_b < T_n < T_{c'}$ is valid. The deformation demand $D = 3.99 \times 5.5803 = 22.29$ cm.

Krawinkler-Nassar Equation (Eq. 19)

For elastoplastic force-deformation behavior, a=1 and b=0.42. Then $c = 0.5 \div (1 + 0.5) + 0.42 \div 0.5 = 1.1733$ (Eq. 20) and $\mu = 1 + (1 \div 1.1733) \times (3.01^{1.1733} - 1) = 3.25$. The deformation demand $D = 3.25 \times 5.5803 = 18.15$ cm.

Vidic-Fajfar-Fischinger Equation (Eq. 22)

Assuming that $T_o = T_c = 0.6634s$ and using the first of the two equations in Eq. (22), gives $\mu = 1 + [0.74 \times (0.6634/0.5)(3.01 - 1)]^{1.053} = 3.05$. The deformation demand $D = 3.05 \times 5.5803 = 17.02$ cm.

SYSTEM 3

Consider an elastoplastic system with the following properties: $T_n = 0.5s$, ζ = 5%, $A_y = f_y \div w = 1.5624g$. The pseudo-acceleration for linear-elastic system with $T_n = 0.5s$, ζ = 5% is $A = 2.7062g$. For this system, $D_y = (2\pi/0.5)^2 \times 1.5624 \times 980 = 9.6962$ cm and $R_y = 2.7062 \div 1.5624 = 1.73$.

Newmark-Hall Equation (Eq. 16)

Assuming that $T_b < T_n < T_{c'}$, gives $\mu = (1 + 1.73^2) \div 2 = 2.0$. For this value of μ, $T_{c'} = 0.6634 \times \sqrt{2 \times 2.0 - 1} / 2.0 = 0.5745$ s and the assumption that $T_b < T_n < T_{c'}$ is valid. The deformation demand $D = 2.0 \times 9.6962 = 19.39$ cm.

Krawinkler-Nassar Equation (Eq. 19)

For elastoplastic force-deformation behavior, a=1 and b=0.42. Then $c = 0.5 \div (1 + 0.5) + 0.42 \div 0.5 = 1.1733$ (Eq. 20) and $\mu = 1 + (1 \div 1.1733) \times (1.73^{1.1733} - 1) = 1.77$. The deformation demand $D = 1.77 \times 9.6962 = 17.20$ cm.

Vidic-Fajfar-Fischinger Equation (Eq. 22)

Assuming that $T_o = T_c = 0.6634s$ and using the first of the two equations in Eq. (22), gives $\mu = 1 + [0.74 \times (0.6634/0.5)(1.73-1)]^{1.053} = 1.71$. The deformation demand $D = 1.71 \times 9.6962 = 16.54$ cm.

SYSTEMS 4 TO 6

Consider an elastoplastic systems with the following properties: $T_n = 1s$, ζ = 5%, $A_y = 0.2997g$, $0.4496g$, and $0.8992g$ for Systems 4, 5, and 6, respectively. The pseudo-acceleration for linear-elastic system with $T_n = 1s$, ζ = 5% is $A = 1.7984g$. For these system, D_y = 7.4403 cm, 11.160 cm, and 22.321 cm, and corresponding values of R_y = 6, 4, and 2.

Newmark-Hall Equation (Eq. 16)

For $T_n > T_c$, $\mu = R_y$ = 6 for System 4, 4 for System 5, and 2 for System 6 which gives $D = \mu \times D_y = 44.64$ cm for all these examples.

Krawinkler-Nassar Equation (Eq. 19)

For elastoplastic force-deformation behavior, a=1 and b=0.42. Then $c = 1.0 \div (1+1.0) + 0.42 \div 1.0 = 0.92$ (Eq. 18). The values of μ for the three Systems are 5.56, 3.80, and 1.97 which give deformation demand D = 41.37 cm, 42.46 cm, and 43.97 cm.

Vidic-Fajfar-Fischinger Equation (Eq. 22)

For $T_n > T_o$, values of μ for the three Systems are 4.97, 3.32, and 1.73 which give deformation demand D = 36.94 cm, 37.0 cm, and 38.58 cm.

The Pacific Earthquake Engineering Research Center (PEER) is a consortium of western U.S. universities working in partnership with business, industry, and government to identify and reduce the risks from major earthquakes to life safety and to the economy.

PEER achieves its objectives of earthquake risk reduction through a coordinated program of research, education, and partnerships with users of research results. PEER's research program includes basic and applied components of seismology, engineering, architecture, urban planning, and economics.

PEER is headquartered at UC Berkeley.

PEER reports are available individually or by yearly subscription from the National Information Service for Earthquake Engineering (NISEE) and from the National Technical Information Service (NTIS).

To order PEER Reports, contact the Pacific Earthquake Engineering Research Center, 1301 S. 46th St., Richmond, California 94804-4698, Tel: 510-231-9468, Fax: 510-231-9461.